# POLITECNICO DI TORINO

**Master's Degree in Electronics engineering**


**Master's Degree Thesis**

# Microfluidic platform development for electrochemical biosensing of cancer biomarkers

**Supervisors**

**Prof. MARZIA QUAGLIO**

**Prof. FRANCESCA FRASCELLA**

**Candidate**

**LORENZO PUCCI**

**July 2021**

**Abstract**

Cancer is one of the leading causes of death worldwide and it is responsible for lowering the average life expectancy, overall in the industrialized world. In particular, lung cancer represents the main cause of cancer death and a relevant pathology with considerable effects on the quality of life of patients and their families, with enormous costs and impacts on society. This is mainly due to the inadequacy of the diagnostic process with respect to the amount and complexity of information to be evaluated by the clinician (e.g. molecular information and its association with clinical and personal information). An early detection of this disease can possibly save many lives, which is why it is important to develop platforms that can make a rapid and reliable diagnosis. Biosensing is based on the detection of analytes thanks to the presence of a recognition element able to generate a specific and detectable signal due to the interaction with the analyte. Several approaches are possible to design a robust biosensor, among them electrochemical biosensing is recognized as one of the most promising being able to directly convert the bio-chemical signal due to the biological event (i.e., the analyte-recognition element interaction) into an electrical one. Given their versatility, electrochemical biosensors can be specifically designed for early stage diagnosis, making them able to identify those biomarkers that are produced at the very starting stage of the target disease. Further improvement of biosensors is possible coupling them to microfluidic platforms. Indeed, the ally of electrochemical biosensors and microfluidic devices can contribute to reduce the volume of reagents, to increase the device sensitivity and to simplify the final protocol, allowing to prepare the sample and to detect the analyte in the same device. Microfluidic approaches coupled with electrochemical techniques for the biosensing allow to transpose the detection from an in the lab to an out of the lab context, increasing therefore the accessibility of the analysis. Indeed, electrochemical techniques do not require trained personnel and guarantee faster response. In this work, a particular focus was placed on Angiopoietin-2 (Ang2), a specific biomarker for lung cancer. A Self-Assembled Monolayer (SAM) was grown on top of a Screen Printed Electrode (SPE) and a specific antibody (a-Ang2) for Ang2 detection was attached on top of it. Furthermore, a microfluidics-based biosensing device was designed with a CAD software and entirely built in polydimethylsiloxane (PDMS). Ang2 concentration was transduced into an electrical signal to be measured and evaluated. This was done thanks to two different electrochemical techniques: Electrochemical Impedance Spectroscopy (EIS) and Square Wave Voltammetry (SWV). In conclusion, after the device was validated trough electrochemical measurements, it was improved

with a new design: device was enlarged, such that more SPEs can be hosted and multiplexed measurements can be carried out in real-time.

# Acknowledgements

Un enorme ringraziamento va a tutte le persone che hanno supervisionato e che mi hanno aiutato durante lo svolgimento della tesi. Senza l'aiuto di Marzia, Francesca, Giulia, Eve, Gianluca e Alessandro non sarebbe stato possibile portare a termine questo lavoro.

Inoltre vorrei ringraziare tutta la famiglia del Chilab. Tutti al suo interno sono stati dei maestri da cui ho cercato di apprendere il più possibile. Ma soprattutto sono e saranno sempre dei grandissimi amici; se in ogni mia futura esperienza troverò un ambiente in cui sarò accolto soltanto la metà di quanto lo sono stato a Chivasso, non dovrò mai lavorare un giorno nella mia vita.

Un ringraziamento va anche a Samuel, Maria e Stefano, supervisori di un progetto che non ha potuto vedere la luce a causa della pandemia. Il loro supporto è stato importantissimo durante i mesi più complicati del 2020.

Grazie a tutti gli amici che hanno condiviso con me questo percorso a Torino e che hanno reso più facile sostenere le ore di lezione al Poli, spesso con lunghi e numerosi aperitivi.

Grazie anche a tutti gli amici in Toscana che mi sostengono ormai da tanti anni in qualunque avventura abbia intrapreso. Penso ormai di aver capito che saremo sempre legati, non importa quello che faccia o quanto lontano mi spinga, so che ci sarà sempre qualcuno ad aspettarmi a casa.

Grazie ai miei compagni di squadra dell'Aquatica per tutte le serate in cui ci siamo presi una birra dopo l'allenamento e soprattutto per avermi fatto diventare un Ingenuotto. Non avremo ancora mai vinto una coppa ma il numero di ristoranti e pub girati dopo ogni partita mi ripaga di ogni sforzo fatto.

Grazie anche a chi, per un motivo o per un altro, ha iniziato con me questo percorso e se ne è andato prima della fine. Devo anche a voi questo risultato e vi ringrazio con tutto il cuore.

Grazie a Ludovica che in questi mesi ha sopportato tutti i miei momenti di crisi e difficoltà quando le cose non sembravano andare per il verso giusto. Ogni volta con il suo sorriso e la sua voglia di vivere mi ha risollevato e mi ha fatto dimenticare ogni problema.

Grazie a tutti i miei nonni per avermi cresciuto con affetto e amandomi ogni

giorno. Spero di avervi reso fieri per la persona che sono diventato.

Infine, grazie ai miei genitori. Non mi avete mai obbligato a fare niente, anzi, mi avete sempre incoraggiato a dare il meglio di me in qualsiasi occasione ma senza nessun tipo di pressione. Ogni scelta che ho preso nella mia vita è sempre stata avallata da voi con il massimo sostegno. Non mi avete mai fatto mancare nulla e posso solo sperare che siate orgogliosi di me. Vi voglio bene.

# Table of Contents

# List of Tables

# List of Figures

# Acronyms

**SAM**
self-assembled monolayer

**LOD**
limit of detection

**QCM**
quartz crystal microbalance

**SWV**
square wave voltammetry

**EIS**
electrochemical impedance spectroscopy

**SPE**
screen printed electrode

**PDMS**
polydimethylsiloxane

**MEMS**
micro-electromechanical systems

**LOC**
lab-on-a-chip

**4-AP**
4-aminophenol

**PA**

paracetamol

**CNT**

carbon nanotube

**SWCNT**

single-walled carbon nanotube

**MWCNT**

multi-walled carbon nanotube

**CCD**

charge-coupled device

**LAS**

Leica application suite

**PMMA**

Poly(methyl methacrylate)

**Ang2**

angiopoietin-2

**a-Ang2**

anti angiopoietin-2

**UPW**

ultra pure water

**FRA**

frequency response analyser

**SC**

small chamber

**BC**

big chamber

**3-MPA**

3-mercapto propionic acid

**PBS**

phosphate-buffered saline

**PBS-t**

phosphate-buffered saline tween

**PDB**

protein data bank

**FC**

functionalization cap

**MC**

measurement cap

# Chapter 1

# Introduction

Cancer is a leading cause of death worldwide, accounting for 19.3 million new cases and 10 million deaths only in 2020. Among the several types of existing cancers, lung cancer is one of the most lethal, with approximately 2.21 million deaths attributed to this particular disease in 2020 [1].

Cancer treatment usually includes radiotherapy and/or chemotherapy which are responsible for many side effects that heavily impact on the quality of life of the patients [2]. For this reason, an early detection of the illness is fundamental in order to treat it with the maximum possible efficiency and with higher probabilities of success [3].

Biosensing offers a great aid from this point of view; when cancer starts developing, alterations of the human body homeostasis result in the overexpression of biomarkers that can be correlated with the onset of the pathology and lead to an early diagnosis. In order to develop a tool able to provide support in the struggle against this disease, a sensing platform to detect biomarkers has been the core work at the basis of this thesis.

In chapter 2 a description of biosensing devices already existing in scientific literature and a theoretical overview of electrochemical biosensing (the type on which this work is based) is provided.

This kind of device is often associated to microfluidics since this field of microtechnology can provide significant advantages like the possibility to integrate on the same platform sample preparation and analysis. All the advantages, together with some examples of recent microfluidic-based devices, are reported in chapter 2.

The rest of this thesis is dedicated to the description of the microfluidic-based device for electrochemical biosensing on which this work is based. The sensing was performed on electrode surface of commercially available sensors.

In chapter 3 a description of all the tools and the materials used for this work can be found. In addition, a theoretical deepening on the electrochemical techniques used to perform measurements is also present.

Chapter 4 is entirely dedicated to the device structure and to measurements results; in the first two sections choices that led to the design and the construction of the device are explained, whereas in the third section the biological protocol that has been followed to functionalize the electrode surface is described in detail. In the end, last section is dedicated to result presentation and discussion.

In chapter 5 an additional design is proposed, based on a new paradigm that allow the development of a more automatized device, in which the interaction with the final user is reduced as much as possible.

Last, in chapter 6, final remarks on this work are made, together with the possible future steps to carry on this project.

# Chapter 2

# State of art

A biosensor is an analytical device, for the detection of an analyte, that combines a biological component (immobilized on a surface) with a physicochemical detector [4], [5].

There are several methods to obtain the immobilization (e.g., adsorption, entrappment, covalent binding) [6]; in this work a Self-Assembled Monolayer (SAM) of thiols was used to anchor the recognition element to a surface.

The recognition element is chosen depending on the target analyte to be detected: e.g., it could be an antibody, an aptamer, a nucleic acid or an enzyme. When the target bounds to the recognition element, a biological signal is generated that must be converted in another physical domain such it can be measured and elaborated [7].

The signal can belong to several physical domains but three major categories can be identified: electrochemical, optical and mass change based [8].

Some analytes absorb or emit light when they bind to the recognition element; optical transducer measure these changes and convert the signal into a quantity that is related to the analyte concentration in a sample. These kind of transducers are widely used because they present many advantages, among them the capacity to perform non-destructive measurements and a low detection limit [9]. Lower detection limit, also known as Limit Of Detection (LOD), is the smallest quantity of a substance that can be recognized with respect to the absence of the same substance [10]; this implies that, the lower the LOD is, the higher is the possibility to detect very small quantities of analyte.

Mass change transducers are based on a different principle, i.e. the change in mass that occurs when the target analyte binds to the recognition element [11]. If a Quartz Crystal Microbalance (QCM) is used, the change in mass implicates a shift in resonance frequency and this quantity is correlated to the analyte concentration [12]. The major reason to use these transducers is that they are very sensitive and they can measure very small changes in mass [13].

Finally, electrochemical transducers are the particular type used in this work; for this reason, section 2.1 is dedicated to their explanation.

## 2.1 Electrochemical biosensing

One of the most common techniques to detect biomolecules is through electrochemistry: this discipline is based on the principle of reduction-oxidation reactions, also known as redox [14].

These chemical reactions are involved when there is an electron transfer; in particular, reduction happens when an electron is gained whereas oxidation happens when an electron is lost [15].

These two processes happen simultaneously, such that there is an electron transfer from the oxidant (the species that loses electrons) to the reductant (the species that gains electrons).

There are several categories of electrochemical methods to measure this electron transfer and to correlate it with analyte concentration. These detection modes are divided into four main groups: coulometric, potentiometric, voltammetic and impedimetric [6].

Coulometry is a technique in which there is a complete electrolysis of the analyte; it is performed keeping the potential or the current constant and the quantity of electric charge, that is consumed or produced, is measured. One of its drawbacks is that the sample is destroyed after the measure [16].

In potentiometry an electric potential between two electrodes is measured; one is called indicator electrode and the other is the reference electrode, fixed at a stable potential. These electrodes are immersed in a solution and, if there is an equilibrium condition, the measured potential coincides with the solution one [17]. In this kind of technique a negligible current flows between the two electrodes. The indicator electrode is usually specific to the target species since an ion-selective membrane is present [18]; its high selectivity is the most important advantage of this technique.

Voltammetry is another category of electroanalytical methods in which electric current is measured whereas potential is varied [19]. Voltammetry is applied on electrochemical cells that can have two or three electrodes; in this work a three electrodes system was used and a more detailed explanation of this structure is given in section 3.1.1. In any case, potential is applied between working and reference electrodes. This technique presents several advantages such as its sensitivity and its high efficiency [20]; furthermore, potential can be varied in several ways, originating many different types of voltammetry. In particular, in this work Square Wave Voltammetry (SWV) was used; theory at its basis is explained in section 3.4.2.

A remark on a particular kind of voltammetry should be done: it is the case

of amperometry. Here, a solution containing electroactive species is put on the working electrode and a fixed potential is applied on the electrochemical cell; when this happens, redox reactions occur at the interface between solution and electrode and a current is measured [21].

Finally, impedimetric methods are based on electrical impedance measurement; a sinusoidal voltage is applied and the response of the system is a sinusoidal current shifted in time with respect to the voltage. The impedance is a complex number obtained from the ratio between voltage and current; indeed, changes in its amplitude and phase give information about the binding between analyte and recognition element [22]. Electrochemical Impedance Spectroscopy (EIS), one of this type of techniques, has been used in this work; more details about can be found in section 3.4.1.

Once explained different forms of detection, it is important to review some of the works that are present in literature in order to highlight which is the state of art in electrochemical biosensing.

Gwon et al. have developed a disposable screen printed electrode sensor for the detection of galactose [23]. They have built their own three electrodes system printing working and reference electrodes on a polyethylene plate and the counter electrode on a separate plate; then, these two layers were put in contact through an adhesive tape. A schematic of the sensor can be seen in Figure 2.1.

Lee et al. built an electrochemical impedance biosensor that employs aptamers as recognition element for a protein label-free detection (Figure 2.2) [24]. Again, they used a Screen Printed Electrode (SPE, that are better explained in section 3.1.1) to perform measurements and they also manufactured it with photolithographic processes to miniaturize it with respect to commercial solutions. Working electrode is made of pyrolized carbon, counter electrode of gold (Au) and reference one consists in a silver (Ag) vertical wire. In addition, a polydimethylsiloxane (PDMS) reservoir was added, surrounding all the electrodes.

Silva et al. fabricated a two electrodes system to set up an electrochemical biosensor for acrylamide detection; acrylamide is a toxic agent widely used in industrial processes [25]. In this case, working electrode is ammonium ion selective whereas reference electrode is a silver/silver chloride (Ag/AgCl) one; they are place on top of two sticks that are completely immersed in the reagents used for functionalization.

In conclusion, Weltin et al. work is shown (Figure 2.3): they developed a flexible microsensor for in vivo detection of glutamate and lactate [26]. Since it has to be inserted inside tissues, the sensor consists on a tip on which a microarray of electrodes is deposited; working and counter electrodes are made of platinum (Pt) whereas reference electrode is Ag/AgCl one.

Except the employment of electrochemical biosensing, all these works have in common the fact that all the sensors that have been used were self-fabricated thanks to cleanroom technologies that allow a considerable degree of freedom when performing functionalization and measurements steps; on the other hand, expensive and complex processes are needed to manufacture the sensors, leading to bigger economical efforts and longer recipe development.
Indeed, in this work a commercial SPE sensor was used; for this reason, there are geometrical constraints that cannot be overcome but there is no need to resort to cleanroom technologies, allowing savings in terms of money and time.
In addition to this, microfluidics is another characteristic present in this work that contributes to take into account several advantages; for this reason, section 2.2 is dedicated to it.

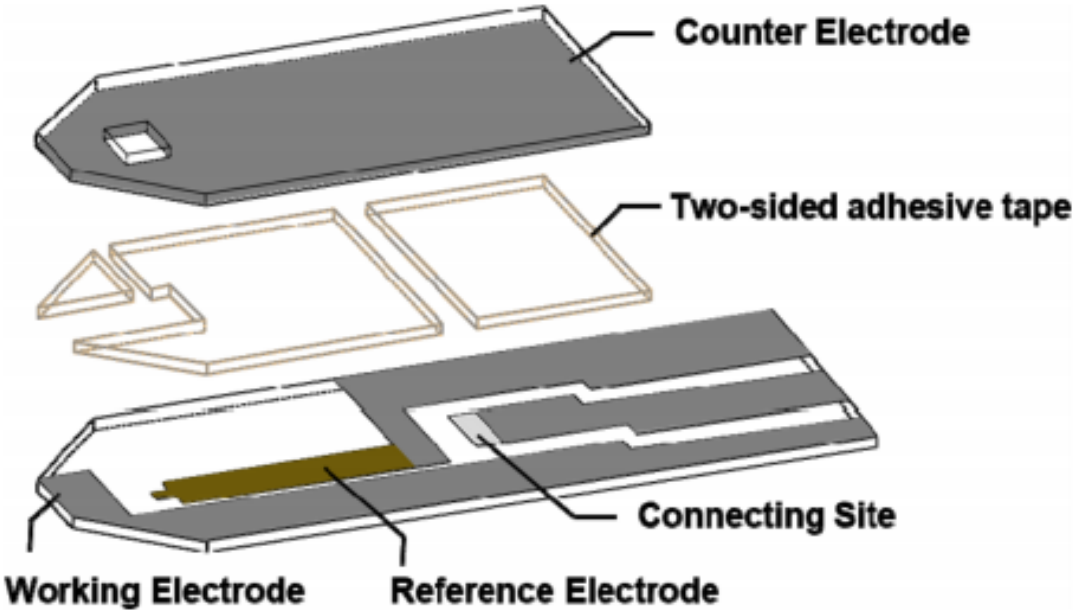


**Figure 2.1:** Disposable screen printed eelctrode sensor for galactose detection, Reprinted from Journal of Electrochemical Science and Technology, Vol 11, Kihak Gwon, Seonhwa Lee, Hakhyun Nam, Jae Ho Shin, Disposable Strip-Type Biosensors for Amperometric Determination of Galactose, 2020

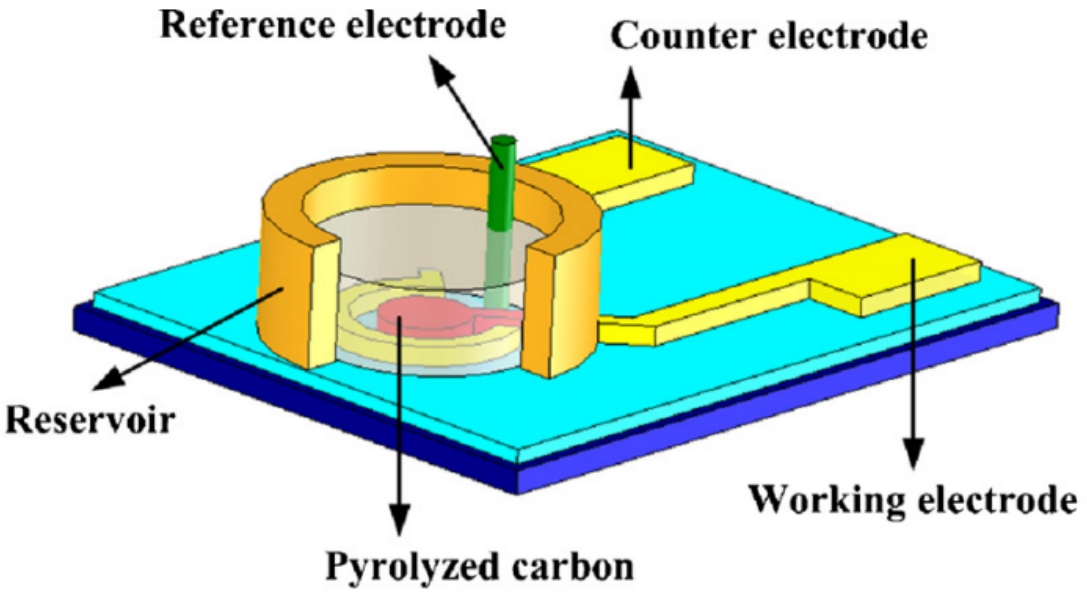


**Figure 2.2:** Electrochemical impedance biosensor for label-free protein detection, Reprinted from Sensors and Actuators B: Chemical, Vol 129, Jung A Lee, Seongpil Hwang Juhyoun Kwak, Se Il Park, Seung S. Lee, Kwang-Cheol Lee, An electrochemical impedance biosensor with aptamer-modified pyrolyzed carbon electrode for label-free protein detection, Copyright (2008), with permission from Elsevier

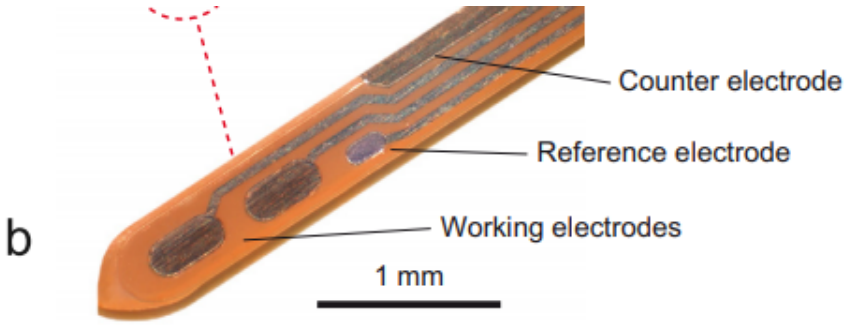


**Figure 2.3:** Flexible microsensor for glutamate and lactate detection, Reprinted from Biosensors and Bioelectronics, Vol 61, Andreas Weltin, Jochen Kieninger, Barbara Enderle, Anne-Kathrin Gellner, Brita Fritsch, Gerald A. Urban, Polymer-based, flexible glutamate and lactate microsensors for in vivo applications, Copyright (2014), with permission from Elsevier

## 2.2 Microfluidics applied to biosensing

In the last fifty years significant improvements have been achieved in the field of miniaturization thanks to the development of new manufacturing techniques [27]: among many achievements, one of the most important has been the birth of Micro-ElectroMechanical Systems (MEMS), devices that combine sensors and transducers from a wide range of physical disciplines and whose dimensions are in the order of $\mu$m [28].

The arise of MEMS opened new paths towards new research topics due to miniaturization and one of them consists in microfluidics, i.e. the study and manufacturing of fluidic systems with channels dimension in the order of $\mu$m and liquid volumes ranging from $\mu$L to pL [29]. Microfluidics provided a great support in the sensing of analytes in the biological field thanks to faster and more sensitive detection methods; furthermore, it allowed sample preparation and analyte detection in the same device, providing a all-in-a-system solution, typical of Lab-on-a-chip (LOC) devices [30]. In addition, microfluidics has led to a reduced economical effort and to more automatized systems and for these reasons has become very popular in recent years [31].

Koh et al developed a wearable microfluidic patch to be applied on skin; it is composed by three layers stacked one on top of the other [32]. First layer is adhesive and it has the functionality to be stuck on user skin; then, second layer is made by PDMS and it hosts all the microfluidic setup. Last, top layer is also made by PDMS but it hosts the electronics to configure the wireless communication between the device and the outer world. This patch analyses sweat samples in situ and it can detect four different analytes; sweat pH, lactate, glucose and chloride. Related microfluidics is of continuous-flow type; this means that the liquid flows continuously and its motion is regulated by mechanical items like pumps [31].

In Figure 2.4 the patch applied on human skin is reported.

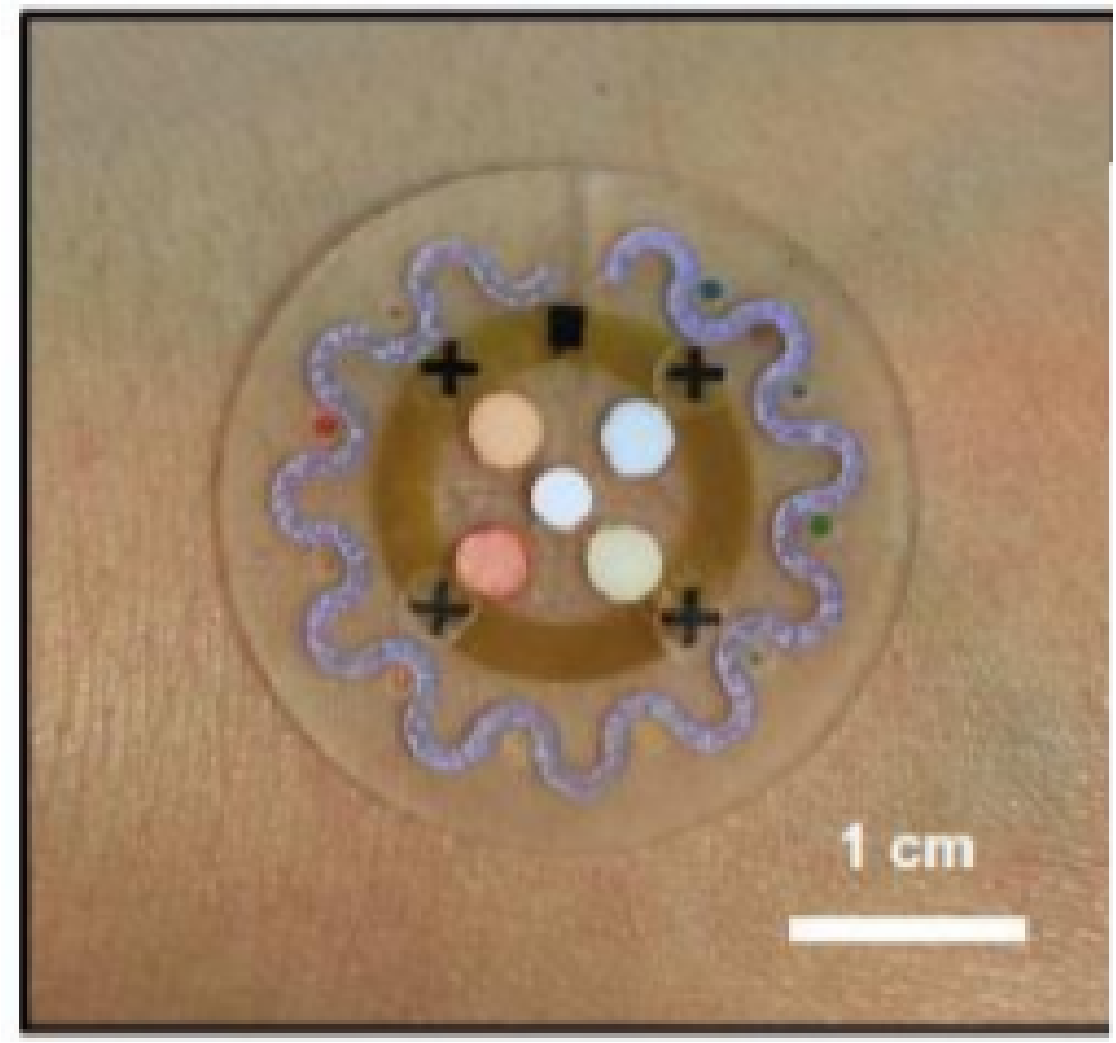


**Figure 2.4:** Wearable microfluidic patch for sweat analysis, From Science Translational Medicine, Vol 8, Ahyeon Koh, Daeshik Kang, Yeguang Xue, Seungmin Lee, Rafal M. Pielak, Jeonghyun Kim, Taehwan Hwang, Seunghwan Min, Anthony Banks, Philippe Bastien, Megan C. Manco, Liang Wang, Kaitlyin R. Ammann, Kyung-In Jang, Phillip Won, Seungyong Han, Roozbeh Ghaffari, Ungyu Paik, Marvin J. Slepian, Guive Balooch, Yonggang Huang, John A. Rogers, A soft, wearable microfluidic device for the capture, storage, and colorimetric sensing of sweat, 2016. Reprinted with permission from AAAS

Another example of continuous-flow microfluidics-based device is given by a cardiac biomarker detector developed by Singh et al [33]. The biosensor is composed

by three electrodes, properly modified to increase device sensitivity to troponin I, a specific indicator of hearth-related problems [34]. As it can be seen in Figure 2.5, all the electrodes pads are contacted by the microfluidic channel; this has contributed to properly functionalize the working electrode and to reach a device sensitivity in the range 0.008−20 ng/mL.

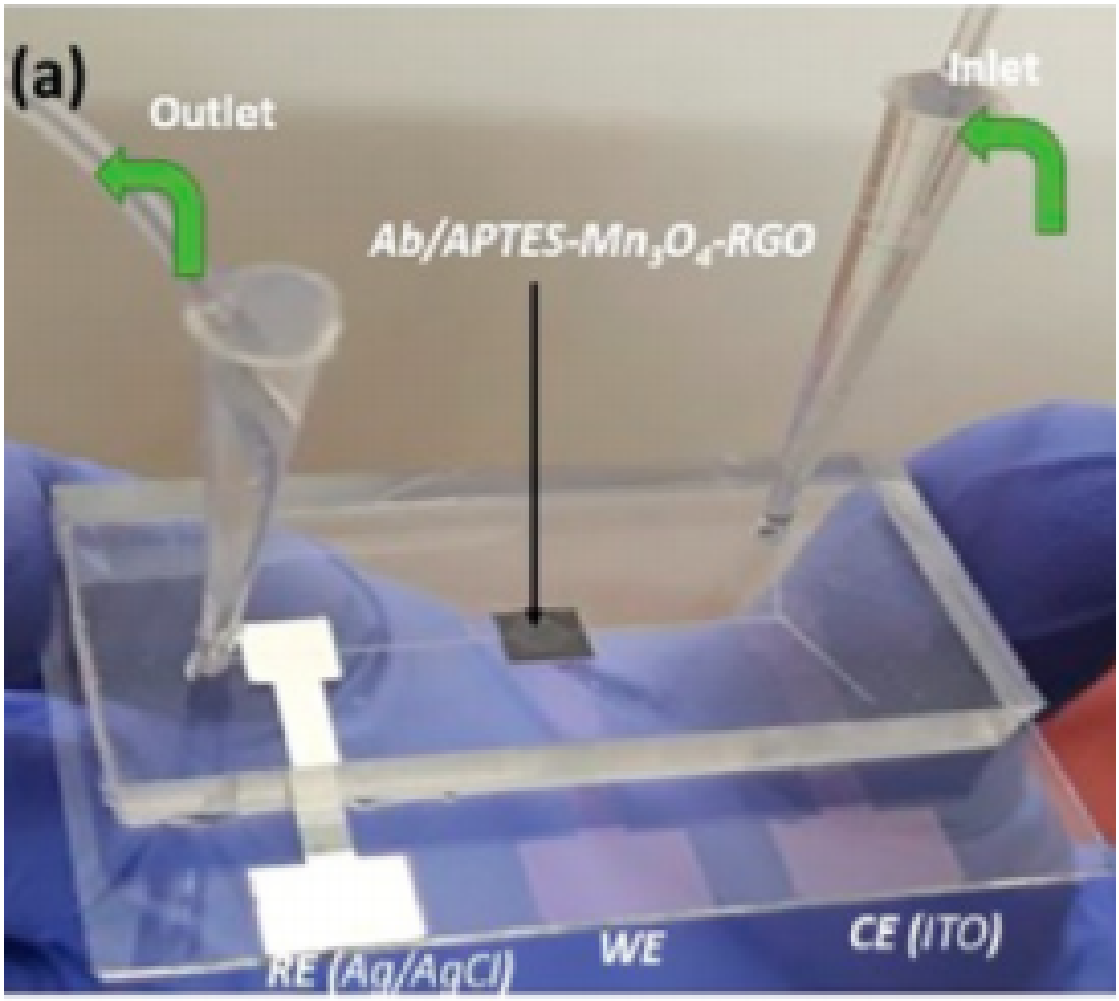


**Figure 2.5:** Cardiac biomarker detector, Reprinted with permission from Applied Materials, Nawab Singh, Md. Azahar Ali, Prabhakar Rai, Ashutosh Sharma, B. D. Malhotra, Renu John, Microporous Nanocomposite Enabled Microfluidic Biochip for Cardiac Biomarker Detection. Copyright (2017) American Chemical Society

To conclude, a work by Rattanarat et al. is shown [35]. In this case a different microfluidic paradigm is applied to the device: droplet-based microfluidics.

In this microfluidic type, liquid flow is no more continuous; instead, liquid of

interest is moved in small portions (droplets) usually separated by a fluid that does not mix with them. Doing this, a discrete flow is obtained instead of a continuous stream [6].

In this case the researchers have developed a microfluidic system for 4-aminophenol (4-AP) detection: this is a possible by-product generated during paracetamol (PA) synthesis and it can be responsible several disease to the human body [36].

The device (reported in Figure 2.6) is formed by two sealed PDMS layers: the bottom one hosts the electrodes and the relative microchannels whereas in the upper layer there are microfluidic channels with inlets and outlets to reach the underlying electrodes.

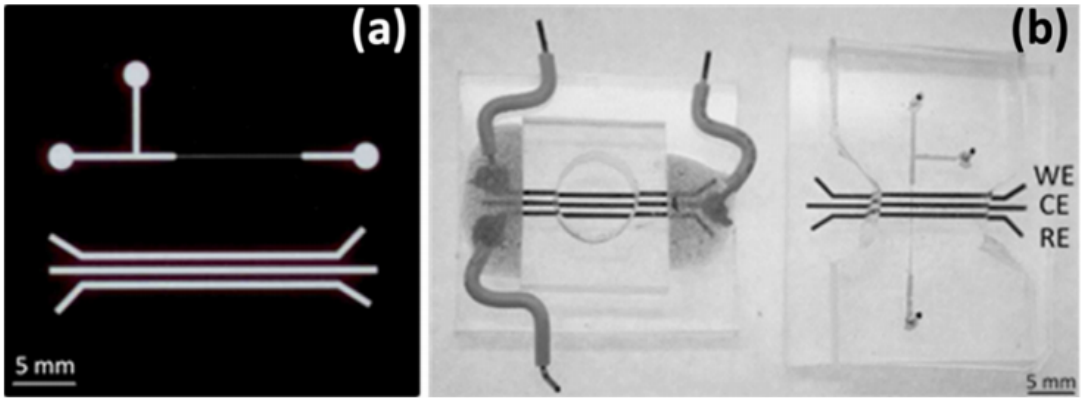


**Figure 2.6:** Microfluidic system for 4-AP detection, Reprinted from Analytica Chimica Acta, Vol 925, Poomrat Rattanarat, Akkapol Suea-Ngam, Nipapan Ruecha, Weena Siangproh, Charles S. Henry, Monpichar Srisa-Art, Orawon Chailapakul, Graphene-polyaniline modified electrochemical droplet-based microfluidic sensor for high-throughput determination of 4-aminophenol, Copyright (2016), with permission from Elsevier

After having seen which are some of the adopted solutions regarding electrochemical biosensing in microfluidics, in the following chapters a deep description of the continuous-flow device present in this work is given: in chapter 4 the detailed procedure used to design and build it is described.

# Chapter 3

# Materials and methods

In this chapter, an overview on all the tools, items, and machines used is reported. In addition, a theoretical deepening on the two electrochemical techniques employed is present.

## 3.1 Device construction

### 3.1.1 Dropsens sensors

The unit at the basis of this work is represented by a commercially available SPE sensor. This kind of device has the peculiarity of having the electrodes printed on a ceramic substrate with an ink that is usually a metal.

SPEs are commonly used in the field of biosensing thanks to their properties: indeed, these sensors are versatile and quite small, and they are also relatively easy to be produced with a little effort in terms of time and money. Among all the advantages obtained by using these kinds of electrodes, SPEs allow implementing the electrochemical measurements in real time, on site and requiring a low consumption of reagents [37], [38].

In this work, SPE have been purchased by Metrohm DropSens, Varese, Italy.

In particular, the model C220AT was used. These sensors have a height of 3.4 cm, a width of 1 cm, a thickness of 0.05 cm. These sensors present 3 electrodes, working electrode, reference electrode and counter electrode, that are screen printed with a concentric circular way onto a ceramic substrate: working and counter electrodes are made by gold (Au) whereas reference electrode and metal stripes (used to put in contact the electrodes with electrical instrumentation from outside world) are made by silver (Ag). In addition, the working electrode has a circular shape and it has a diameter of 4 mm.

In Figure 3.1 it is represented the sensor model used in this work;


**Figure 3.1:** Screen printed electrode manufactured by Sensonor

As mainly explored in several works in the literature, the function of these 3 electrodes were deeply investigated. Onto the working electrode, the electrochemical reaction occurs; furthermore, this is the surface that is functionalized in order to detect target analyte. Then, the function of reference electrode is to achieve a defined and stable potential such that all the potentials in the circuit are measured with respect to it. Last, counter electrode or auxiliary electrode plays a crucial role to electrically close the circuit, preventing current to flow in working electrode, in order not to alter its potential. On this electrode no electrochemical reaction takes place.

### 3.1.2 Carbon nanotubes

As will be explained in section 4.2, carbon nanotubes (CNT) were mixed with PDMS to produce electrical contacts suitable to perform the electrochemical characteriations and able to ensure good mechanical robustness.

CNT are tubes made of carbon that have a diameter in order of nm and they can be split in two groups: Single-Walled Carbon NanoTube (SWCNT) and Multi-Walled Carbon NanoTube (MWCNT). SWCNTs are made by a single graphitic foil wrapped in a cylindric way whereas in MWCNTs there are multiple foils coaxially wrapped one on the other.

CNTs present several interesting characteristics such as good mechanical and

thermal properties but the one of major interest for the aim of this thesis are the electric ones [39], [40]; indeed, they can bear very high current densities [41] and they can have a conductor or semiconductor behaviour (depending on chirality); chirality can be defined as the impossibility to match an object and its mirror image with operation of translation and rotation [42].

In this work, MWCNTs purchased Nanocyl by were used.

### 3.1.3 Digital microscope

A digital microscope was employed to take pictures and video of the sensors electrodes: this was done while testing the microfluidics in order to verify the absence of liquid leakages in the device and its correct functioning in terms of chambers filling.

Digital microscope DVM2500 was purchased by Leica; it is equipped with a Charge-Coupled Device (CCD) of 2.11 Megapixels and trough the dedicated software Leica Application Suite (LAS) it is possible to process and to elaborate images.

In addition, it was provided with a camera lens (model VZ 80 C) that is able to zoom the picture up to 400 times.

### 3.1.4 Oxygen plasma bonding

Oxygen plasma bonding is the technique that has been employed to attach the four PDMS layer that form the device. Plasma is one of the fundamental states of matter and it consists in a mix of electrons, molecules (ionized, excited, neutral), ions and free radicals (very reactive and neutral species) [43]. Among several different applications, plasma is widely used to clean surfaces from impurities [44], and this is the reason it was used in this work.

Plasma bonding was defined by putting each PDMS layer into the chamber. The initial pressure was set at 0.30 mbar and once reached this value of pressure, gas ($O_2$ in this case) is supplied for 1 minute and the internal pressure rises to 0.60 mbar. Plasma is produced for 30 seconds; during this latter process, the oxygen plasma was able to remove all organic impurities on PDMS layer, inducing the formation of silanol (SiOH) groups exposed onto the PDMS surface. These latter groups guarantees the bonding of different layers, since when the two treated surfaces were put in contact, a Si-O-Si bonding is formed.

### 3.1.5 Laser ablation

Laser ablation is a technique that is used to remove material from a surface by heating it locally with a laser beam; among its wide application range it is well

known in the biomedical field because it is used in surgery to burn tissues [45].

In the present work laser ablation machine has been used to produce the PMMA (Poly(methyl methacrylate)) molds that have been filled with PDMS; in principle, it would have been possible to draw the required shapes of PDMS layers (that will be described in section 4.1) directly with the laser ablation machine but the process would have been very complex due to the fact that its software only allows to reproduce very simple geometrical figures.

For this reason, CAD Rhinoceros was used to obtain drawings with a dxf extension, the one that must be provided to the machine as input. The only limitation, as previously reported, is that the working area that cannot exceed 49 $cm^2$.

Even if there is a limitation on allowed dimensions, laser ablation machine is still advantageous with respect to other techniques used to build microfluidic devices; indeed, resolution is higher with respect to the one that can be obtained with mechanical tools like milling machine and this leads to the production of smaller features. Then, the molds may be produced with a 3D printing machine instead of being dug in PMMA sheets; but this technique would be slower with respect to laser ablation, besides being a too expensive choice for a mold whose function is only to be filled with PDMS.

In order to employ a suitable laser ablation, several parameters can be defined, such as power, frequency, scan speed and the number of scan repetition. The energy induced onto PMMA substrate is strictly correlated with the power and frequency of laser emission REF. Moreover, several experiments done with this technique allow defining how the final depth of the mold results to be a function of the combination of above-mentioned parameters. The final result is reported in table 3.1.

| Parameters | Value | Unit |
|---|---|---|
| Power | 30 | W |
| Frequency | 2000 | Hz |
| Beam angle | 45 | ° |
| Scan speed | 75 | mm/s |
| Number of repetitions | 3 | dimensionless |

**Table 3.1:** Laser ablation machine parameters

In the case of this project, all the layers required approximately 30 minutes of work each.

## 3.2 Functionalization

### 3.2.1 Angiopoietin-2

Angiopoietins are a group of secreted factors that are involved in angiogenesis; this is a natural process that allows the formation of new veins and capillaries [46]. Angiogenesis is normally present in case of tissues healing, but it can also be an indicator of a cancer formation; indeed, a developing cancer needs blood supply in order to favour its grown and metastasis formation [47].

Among the four different angiopoietin types, this work has been focused on Angiopoietin-2 (Ang2); it is a protein that inhibits the angiogenesis and therefore its production is very often related to cancer inflammations [48]. This means that a measure of its concentration in human body can provide information about the presence of this disease, giving the opportunity to treat it properly before a too extended growth [49].

A recent study conducted on hospitalized patients affected by COVID-19 also correlates Ang2 concentration with more severe forms of this disease; in particular Ang2 concentration measured after three days in hospital gives indication on which patients have a higher probability of mortality, whereas concentration after ten days can be a symptom of chronicle lung disorder [50].

As already explained in chapter 2, Ang2 plays the role of target analyte; to produce a biological signal it has to be linked to a recognition element, usually a specific antibody (here Anti Angiopoietin-2, a-Ang2). Both Ang2 and a-Ang2 were purchased by R&D systems.

## 3.3 Electrochemical measurements

### 3.3.1 Potassium ferrocyanide and potassium ferricyanide

In order to perform electrochemical measurements, a water-based solution containing potassium hexacyanoferrate-II ($K_4[Fe(CN)_6]$) and potassium hexacyanoferrate-III ($K_3[Fe(CN)_6]$) was used; these two reagents were purchased by Sigma Aldrich and they have the function of redox couple.

$K_3[Fe(CN)_6$ and $K_4[Fe(CN)_6]$ are respectively a dark red solid and a yellow powder at room temperature; among their characteristics, it is important to underline their low toxicity [51] and their solubility in water [52].

Indeed, the final solution used to perform measurements contained 5mM of both components in UPW.

### 3.3.2 Palmsens

Palmens 4 is the device used to perform measurements on Dropsens sensors: it is a potentiostat, galvanostat and Frequency Response Analyser (FRA) that, among the numerous techniques at its disposal, can run Electrochemical Impedance Spectroscopy (EIS) and Square Wave Voltammetry(SWV) which are of interest in this work.


**Figure 3.2:** Palmsens4 potentiostat

Palmsens 4 presents a potential range from -5 V to 5 V, a current range from 100 pA to 10 mA and a maximum EIS frequency of 100 kHz. It provides the output

for device pads through a double shielded cell cable with crocodile clips whereas input parameters are configured from the software PSTrace (version 5.8); Palmsens 4 and laptop are connected through a USB cable.

As just mentioned, PSTrace is used to set specifications for the two techniques that were employed in this work; a better understanding of these inputs will be given in sections 3.4.1 and 3.4.2 respectively related to EIS and SWV.

## 3.4 Electrochemical techniques

### 3.4.1 EIS

Electrochemical Impedance Spectroscopy (EIS) is a quite complex but extensively applied technique in the field of electrochemistry; as the name suggests, impedance is the main concept at its foundations [53].

Impedance is defined as expressed by equation 3.1:

$$Z = \frac{V}{I} \tag{3.1}$$

Where Z is the impedance value ($\Omega$), V is the voltage across the system (V) and I is the current that flows into the system (A). The impedance Z can be also defined as an equivalent of electric resistance in AC systems; it is also a complex number, therefore it can be expressed through in polar coordinates, as reported in equation 3.2:

$$\rho = e^{i\theta} \tag{3.2}$$

where i is the imaginary unit, module ($\rho$) and phase ($\theta$).

When EIS is performed, AC voltage at a given frequency is applied; the response will be an electric current at the same frequency but shifted in time. The quantity that takes into account this phenomenon is called phase shift [54].

Considering what is stated above and according to (3.1) also Z is frequency dependent. In particular, this is true for reactive circuit elements like capacitors and inductors; indeed, in the case of resistors, electrical impedance and electrical resistance are the same as stated in equation 3.3

$$Z_R = R \tag{3.3}$$

and this means that voltage and current are in phase.

Formulas for computing impedance for capacitors and inductors are expressed in equations 3.4 and 3.5:

$$Z_C = \frac{1}{i\omega C} \tag{3.4}$$

$$Z_L = i\omega L \tag{3.5}$$

In this case voltage and current are shifted by +90° and -90° respectively.

Thus, the result obtained when performing EIS, is a set of impedance values, one for each different frequency of AC voltage applied; these values are usually represented in two different graphs: Bode plot and Nyquist plot [55]

In Bode plot both impedance magnitude and phase are represented with respect to frequency whereas in Nyquist plot real and (negative) imaginary parts are represented on x and y axis respectively.

These two plots show different characteristics: Bode plot represents at the same time two magnitudes and it also provides frequency information. On the other hand, each point on Nyquist plot represents the impedance value at a given frequency even if this frequency cannot be established looking at the graph.

Furthermore, being the impedance a complex number, each point on Nyquist plot can be represented using polar coordinates: if the point is connected to the axis origin with a vector, the vector length will represent impedance modulus whereas the angle that is formed between x axis and the vector itself will represent the phase.

In any case, both plots are used in the scientific community but in this work the focus was placed on Nyquist plot, being the one more diffused in literature for the study of solid-liquid interfaces in EIS [56]; in addition, as it will be explained in the following of this section, Nyquist plot is very useful to look separately at the physical processes that happen during EIS.

To interpret this plot an equivalent electric circuit was used [57]; its name is Randles circuit and it is reported in Figure 3.3.

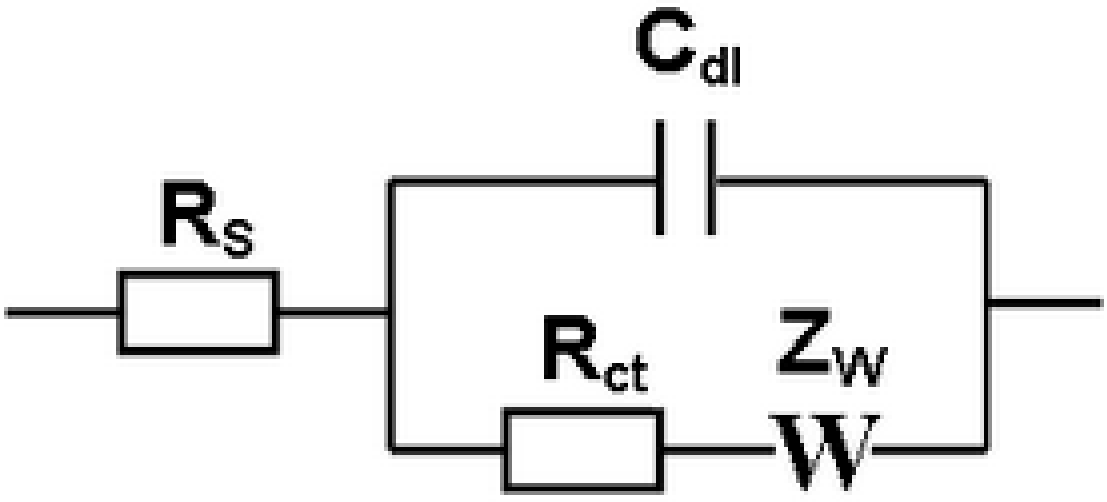


**Figure 3.3:** Randles circuit

Each element in the circuit represents a physical phenomenon that takes place during redox reactions of the solution involved in the measurements (see 3.3.1): $R_s$ takes into account electrolyte resistance, $R_{ct}$ is the charge transfer resistance, $C_{dl}$ is the electrical double layer capacitance (structure at the interface solid-liquid where a charge transfer is present) and $Z_W$ is the Warburg element (used to model diffusion process).

$R_s$ depends on many factor such as temperature, ionic concentration, type of ions and electrodes geometry; since these parameters are variegated, it would be very difficult to calculate $R_s$ in an analytical way; instead, it is determined by fitting experimental data into a model like Randles circuit.

To explain $R_{ct}$ it must be considered that when a metal substrate (electrode surface in this case) and an electrolyte are in contact, the metal can dissolve electrolytically into the electrolyte. There is a charge transfer because metal ions diffuse into the electrolyte whereas electrons from electrolyte enter into the metal.

This behaviour is explained through a quite complex equation that simplifies when the concentrations of oxidant and reductant species at electrode surface and in the bulk are the same.

In this case, current-potential relation follows formula 3.6 called Butler-Volmer equation:

$$I = I_0 * e(\frac{\alpha n F \eta}{RT}) - e(\frac{-(1-\alpha) n F \eta}{RT}) \tag{3.6}$$

where $I_0$ is the exchange current density, $\alpha$ is the reaction order, n is the number of electrons involved, F is Faraday constant, $\eta$ is the overpotential (difference between applied potential and open circuit potential), R is gas constant and T is the temperature [58].

When $\eta$ is very small, the system is at equilibrium and we can easily calculate $R_{ct}$ using equation 3.7:

$$R_{ct} = \frac{RT}{nFI_0} \tag{3.7}$$

$C_{dl}$ represents the physical phenomenon of electrical double layer: when a metal and an electrolyte are put in contact, ions from electrolyte tend to be adsorbed by the mtal that, for this reason, will be charged. Furthermore, metal surface and electrolyte (that contain charged ions) are separated by a very thin insulator layer, in the order of Å; this leads to model this effect with $C_{dl}$ since a capacitor is formed by two charged surfaces separated by an insulator.

Finally, $Z_W$ is the element that takes into account diffusion; this parameter originates a line with a slope of 45° in Nyquist plot.

Equations that rule Warburg impedance are complex but they can be simplified at low frequency if the diffusion layer is not infinite [59]. Indeed, the relation is

expressed in equation 3.8:

$$Z_W = \sigma\omega^{-\frac{1}{2}}(1-i)\tanh(\delta(\frac{i\omega}{D})^{\frac{1}{2}}) \tag{3.8}$$

where $\sigma$ is the Warburg coefficient, $\omega$ is the angular frequency, i is the imaginary unit, $\delta$ is Nerst diffusion layer thickness and D is a parameter related to diffusion coefficient of the diffusing species.

In Figure 3.4, taken by [60], it can be seen an ideal Nyquist plot whose interpretation is given by Randles circuit.

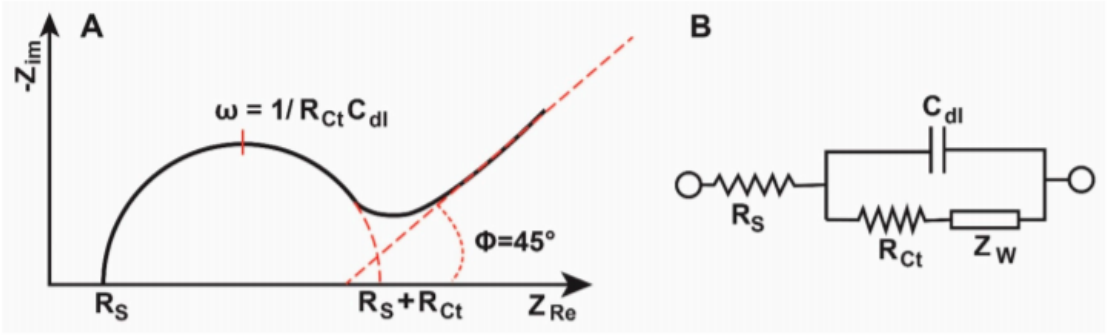


**Figure 3.4:** Nyquist plot and Randles circuit, Reprinted from Micromachines, Vol 11, Niazul I. Khan, Edward Song, Lab-on-a-Chip Systems for Aptamer-Based Biosensing, 2020

A particular of Nyquist plot is that points on the left (closer to the origin) are taken at high frequencies whereas points on the right are taken at low frequencies; this means that, looking at different parts of the plot, we can acquire different information. Indeed, at low frequencies all the physical processes are present because they have enough time to happen; on the contrary, when frequency is higher, slower processes like diffusion are not visible.

At high frequencies, i.e. for $\omega\to+\infty$, $Z_C\to0$, according to (3.4); therefore, the equivalent circuit is composed only by $R_{sol}$.

On the contrary, for $\omega\to0$, $Z_C\to+\infty$ and the equivalent circuit is the series of $R_s$, $R_{ct}$ and $Z_W$; this is the mathematical explanation of the presence of diffusion only at low frequencies.

In this work, the applied parameters to perform EIS have been 0 V DC voltage and 0.01 V AC voltage with a frequency scan of 41 different points, ranging from 50 kHz to 5 mHz.

Data were fitted in a equivalent Randles circuit (whose structure was explained above) thanks to the software EIS Spectrum Analyser; values of Randles circuit component were imported in MATLAB and plotted with error bars calculation based on the least square method.

### 3.4.2 SWV

Square Wave Voltammetry (SWV) is one of the techniques that belong to the field of voltammetry: in this category a potential sweep is applied to a device containing an analyte while electric current is measured as output.

In particular, in SWV voltage sweep is the result of a superposition of a square wave (with fixed amplitude and frequency) and a staircase potential; potential is applied between working and reference electrodes whereas resulting current is measured at working electrode.

A square wave has maximum and minimum voltage values (also called high and low levels) that define its amplitude; therefore it switches between these two values at a given frequency.

In this work, the following parameters were settled: for the staircase a potential ranging from -0.2 V to 0.6 V with a step of 0.01 V was applied; square wave amplitude was 0.05 V and its frequency was 25 Hz.

The current is sampled two times per cycle, just before the transition between high and low (or viceversa); this means that two current values are obtained, one measured when potential is high (forward current) and the other measured when potential is low (reverse current).

Usually, instead of a double plot, difference between the two current with respect to applied staircase potential is plotted. The most meaningful aspect of this plot is current peak ($\Delta i_p$) which gives information about analyte concentration thanks to redox reactions that take place at the interface between electrode and liquid solution.

Current peak can be also analytically determined using Cottrell equation:

$$\Delta i_p = \frac{nFAc_j^O\sqrt{D_j}}{\sqrt{\pi}t} \tag{3.9}$$

where n is the number of electrons to reduce or oxidize a molecule of the analyte, F is Faraday constant, A is the area of the planar electrode, $c_j^0$ is the initial concentration of the analyte, $D_j$ is the diffusion coefficient and t is the time.

# Chapter 4

# First device design and measurements

## 4.1 Device design

In chapter 2, some of the techniques, which represent the state of the art in the field of electrochemical biosensing, were illustrated. In this thesis, the functionalization steps were performed only on the working electrode's surface, whereas the electrical measurements also involve counter and reference ones. The electrodes' arrangement and their specific geometry resulted to be crucial in determining the project choices; indeed, during the development of this work, the concentric disposition of the electrodes was the main aspect that influenced the device's design.

Since the functionalization step and the electrochemical measurements must be conducted in a separate environment, the design of two concentric chambers, placed on top of the electrodes that are accessible separately, plays a crucial role to achieve one of the aim of this work.

These 2 chambers can be defined as *i)* small chamber (SC) that provides access to the working electrode for functionalizing it; *ii)* big chamber (BC) that guarantees that all electrodes can be reached by the electrolyte during electrochemical measurements.

The two chambers are physically separated by a PDMS barrier such that liquids involved in functionalization are not able to wet auxiliary and reference electrodes. For this reason, two sets of microfluidic channels are also needed: one that serves the SC and the other that gives access to the BC.

Besides their target chamber, they can be also divided in inlet or outlet channels (even if some of them accomplish both these functions); to better clarify this concept, it can be useful to take a look to the CAD files used to project the device.

The device's design was realized using a CAD software called Rhinoceros; this

software gives the possibility to draw 2D and 3D models. In our case a 2D drawing was implemented to produce a pattern that had to be dug on a PMMA surface by a laser ablation machine. PMMA is a transparent thermoplastic material, and it is commonly known with the name of Plexiglas; it is selected due to its biocompatible properties and its low cost [61], [62]. PMMA was cleaned with isopropanol before the laser ablation process. More details about this topic can be found in chapter 3.

To design the device for functionalization and electrochemical measurements, four CAD files were drawn. Each file represents different layers of the whole device. Figure 4.1 represents the bottom part, which is the basis of the device, and it reports 3 slots dedicated for 3 different electrochemical sensors. The geometric area is close to 49 $cm^2$. This value has been selected in order to overcome the limit imposed by laser ablation machine that is used to dig the PMMA sheet.

On the basis part a first layer was placed. This layer hosts the microfluidic channel, directly connected with the working electrode. These channels were used both as inlets and outlets, as represented in Figure 4.2.

Figure 4.3 represents the second layer used only to define the contour of the big chamber that include also the small one.

A third layer was designed with the main purpose to define the set of microfluidic channels useful for filling the big chamber, covering all electrodes at the same time. Moreover, this layer was also implemented to form a sort of well, since it closes the top of the two chambers, small and big chambers. The 2D model for this layer is sketched in Figure 4.4; it can be seen that each sensor is served by two channels. This is a form of redundancy because, depending on the protocol step to be implemented (explained in detail in section 4.3), the same channel can be used at the same time as input and output or one channel can serve as an input and the other as on output.

The presence of two channels was suitable to overcome the limit imposed by the presence of air in the chambers when the devices are empty. Indeed, when the solution, acted as electrolyte, is introduced inside the chamber, the second channel acts as venting hole for the air present inside the chamber.

In conclusion, the conceived device results in the stacking of three different functional layers hosting the microfluidics and a fourth one, on the basis, (hosting the sensors). As a final remark, in all layers, the inlet of the small chamber channel has been realized because it is a through hole, and it must be reached from outside world. This is not the case of the big chamber channels, because they are built inside the third layer, and they are already on top of the device.

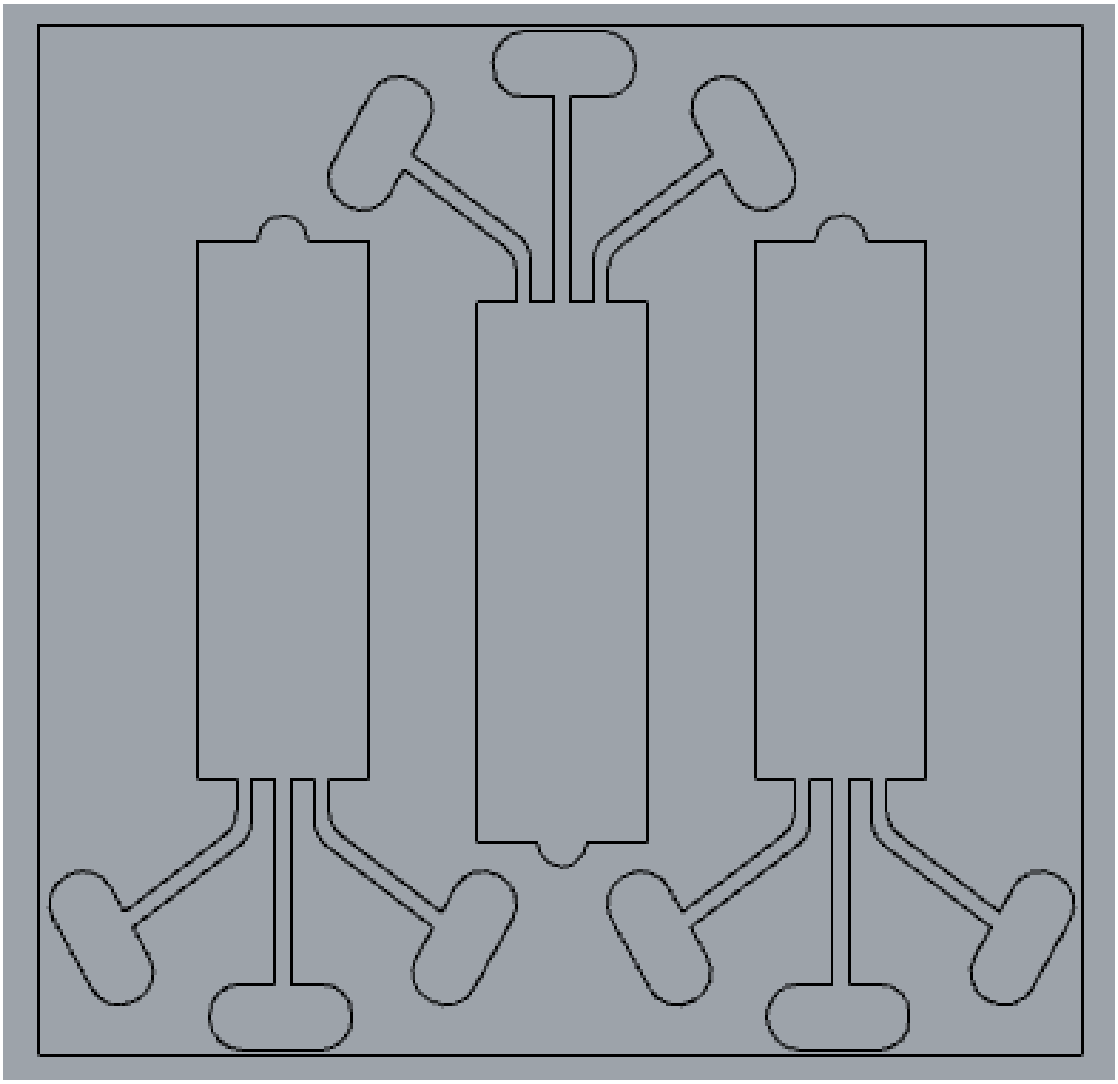

**Figure 4.1:** CAD for device basis

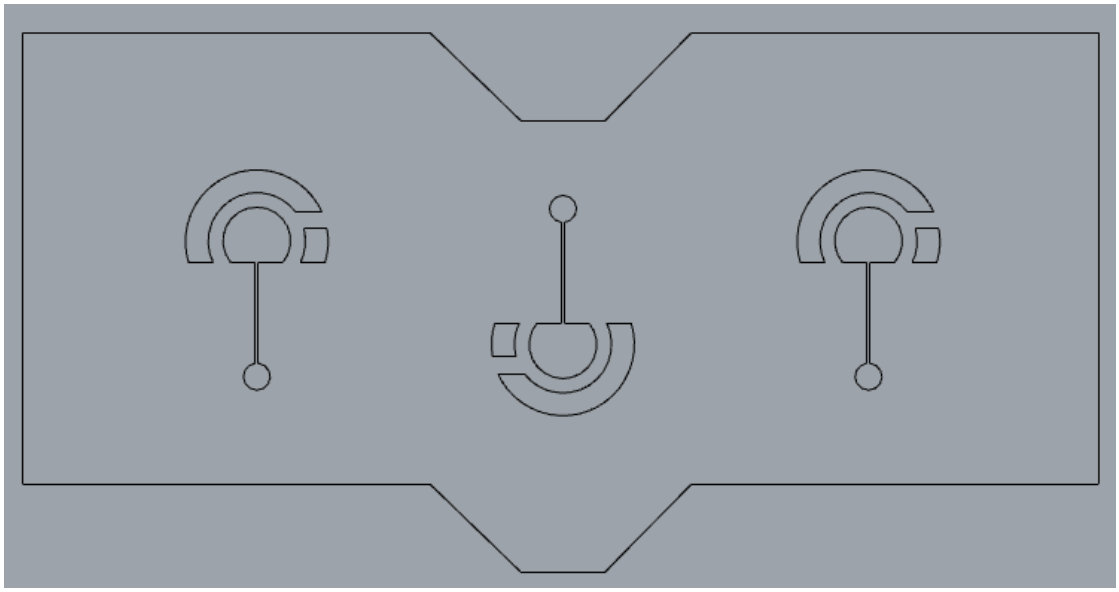

**Figure 4.2:** CAD for first layer

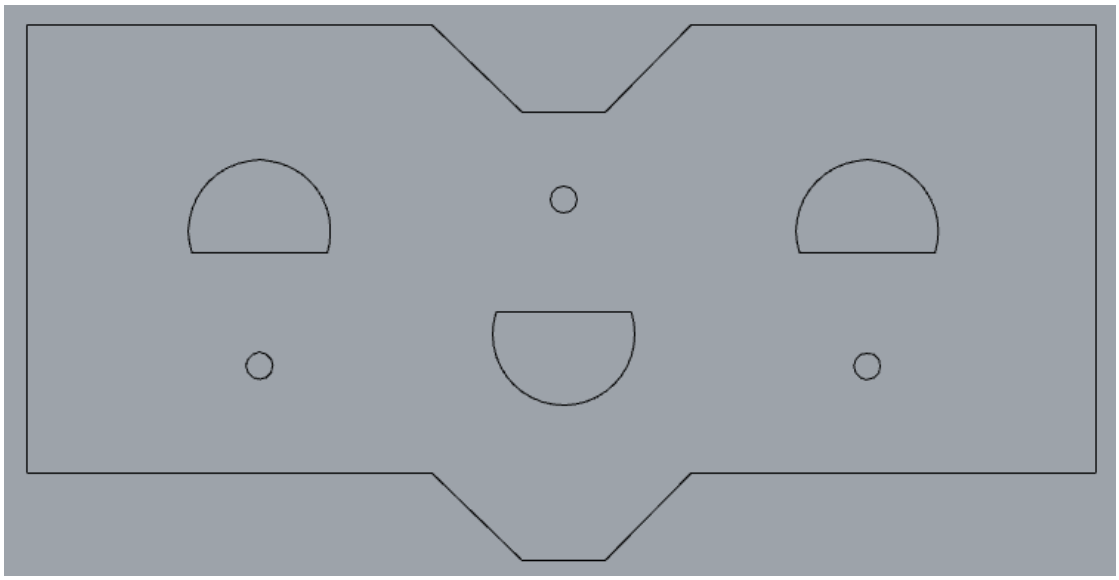

**Figure 4.3:** CAD for second layer

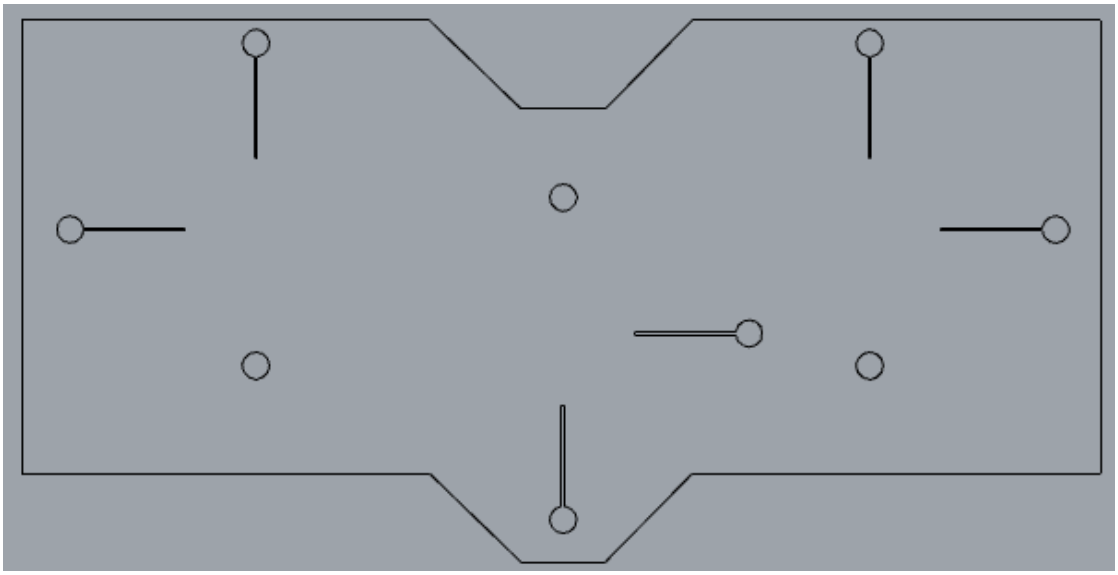

**Figure 4.4:** CAD for third layer

## 4.2 Device fabrication

The whole device is made of PDMS. As stated by several works in the literature, PDMS was selected thank to its intrinsic properties, such as biocompatibility, low cost, flexibility, optically transparent and easily fabricated material [63]. In particular in this thesis, the optically transparent properties result to be pivotal to have a good overview of the steps involving microfluidics since it grants a quick troubleshooting.

PDMS is an organic polymer based on silicone that is obtained mixing a resin and a curing agent with a well-defined ratio. This ratio affects mechanical and physical properties of PDMS such as its density and the Young modulus; in particular, Figure 4.5 represents how the density approximately grows in a linear way with the amount of resin whereas Young modulus value also depends on the temperature and on the amount of time at which PDMS is cured (see Figure 4.6).

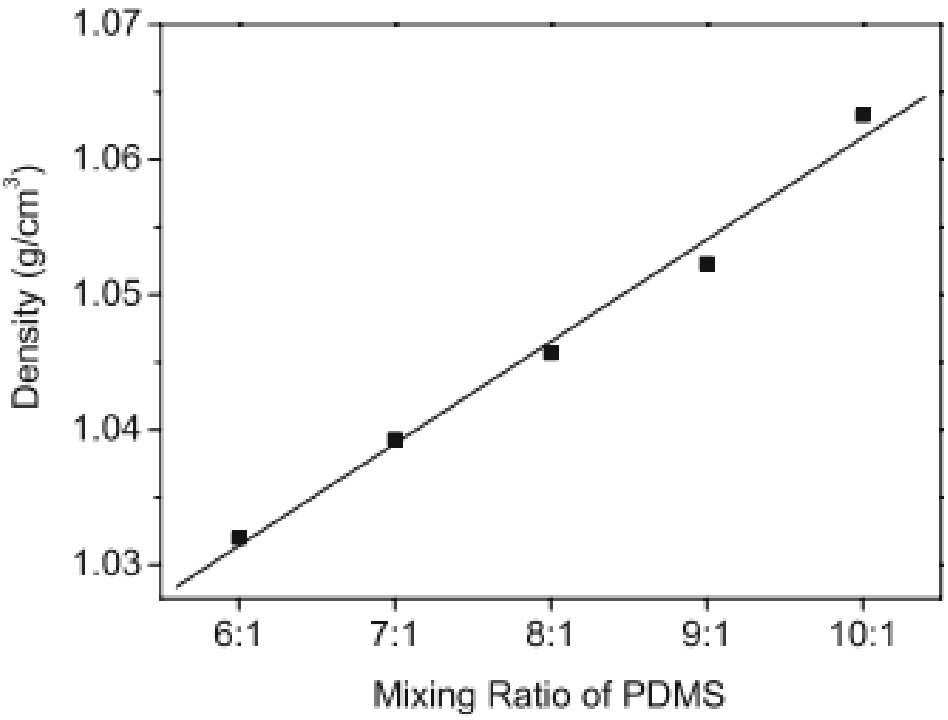


**Figure 4.5:** Relation between PDMS mixing ratio and its density, Reprinted by permission from Springer Nature: Nature Springer, Microsystem Technologies, Study of novel electrical routing and integrated packaging on bio-compatible flexible substrates, Hong Hocheng, Chao-Ming Chen, Yu-Chang Chou, Chien-Hung Lin, Copyright (2009)

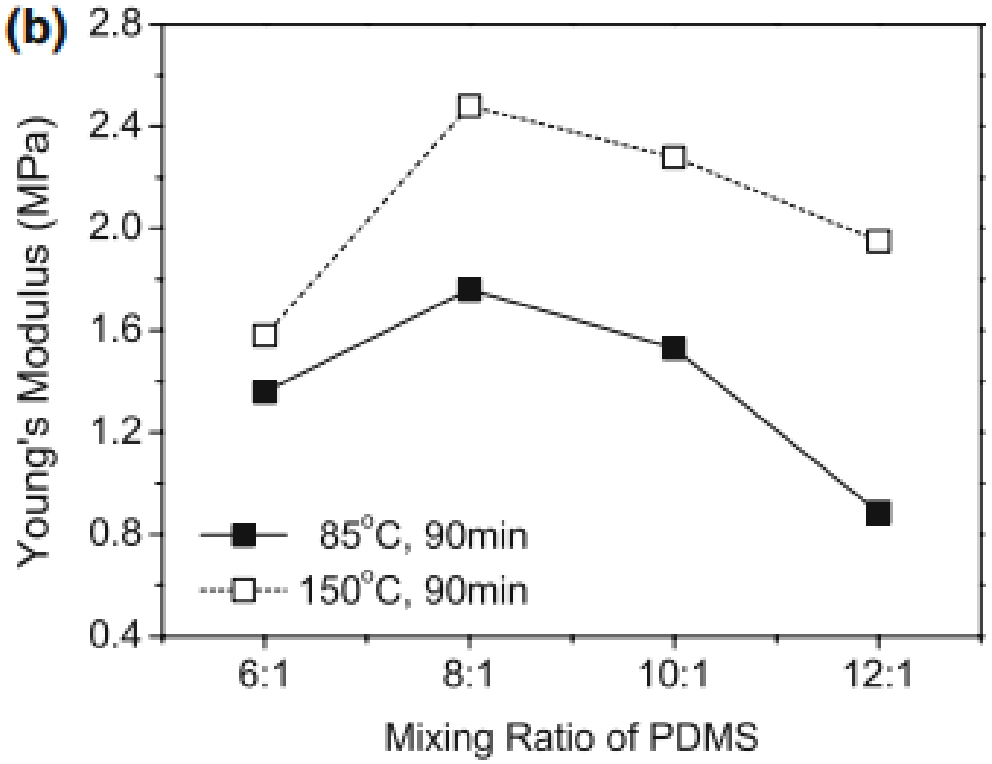


**Figure 4.6:** Relation between PDMS mixing ratio and its Young modulus, Reprinted by permission from Springer Nature: Nature Springer, Microsystem Technologies, Study of novel electrical routing and integrated packaging on bio-compatible flexible substrates, Hong Hocheng, Chao-Ming Chen, Yu-Chang Chou, Chien-Hung Lin, Copyright (2009)

In this work, 10:1 ratio was used. To eliminate all the air bubbles that may affect the quality of PDMS, the glass was put inside a vacuum pump for about 15 minutes. After this step, PDMS was poured inside four different PMMA molds and put them in an oven at a temperature of 85°C for 90 minutes. Since PMMA melting point is at a temperature of 160°C, there was no risk of destroying the molds [64].

As explained in the previous section, four PMMA molds correspond to four PDMS layers, one for the device basis and the other three stacked on its top. The practical building starts from the bottom for easiness of layers alignment.

As an example, in Figure 4.7 device basis is reported; three sensors fit in this area and on each sensor, the biological functionalization protocol was applied onto working electrodes required for the subsequent electrochemical measurements. This concept will be better explained in section 4.3.

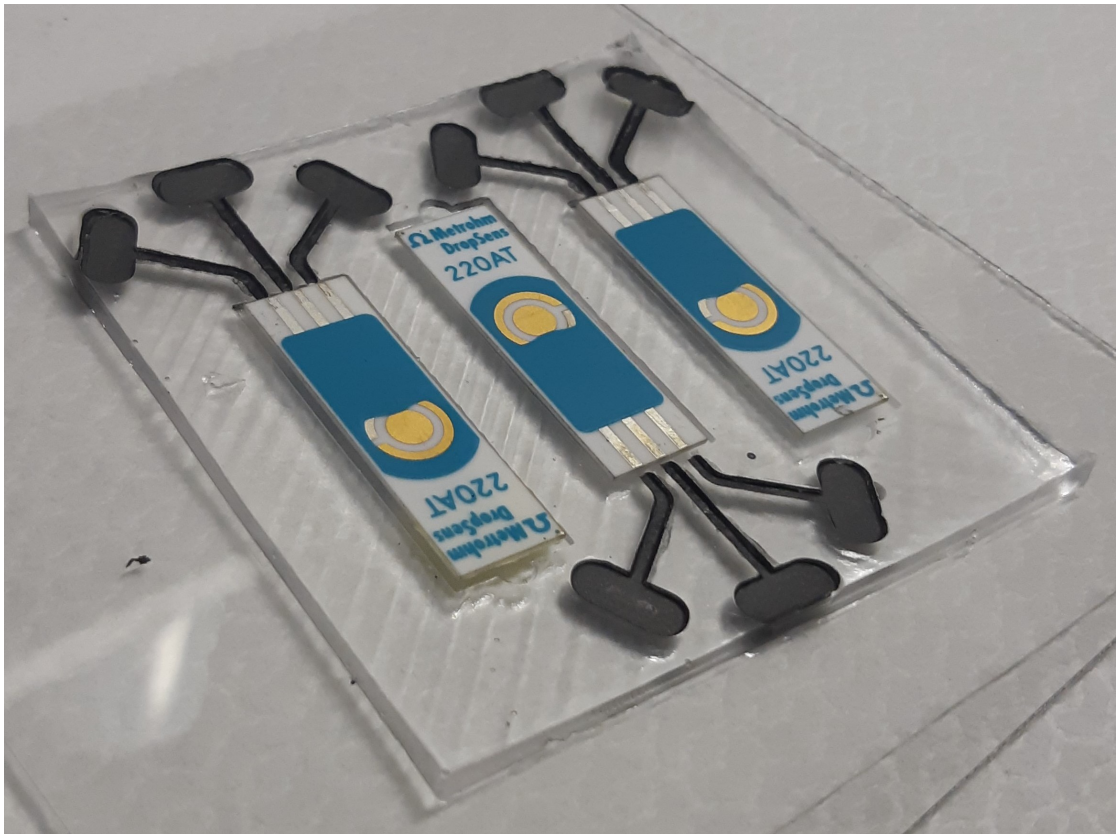


**Figure 4.7:** Device basis with three sensor slots

The device basis also contains interconnections between itself and the outer world: indeed, there are paths and pads that have been filled with carbon-based paste to ensure proper electrical contacts and a good mechanical resistance.

In particular regarding the paths, since it was difficult to develop a proper electrical contact with the metal stripes of SPEs, preventing and avoiding short circuits between all electrodes of SPEs, a bridge of solid carbon cement (purchased from Leit-C) was used for ensuring electrical contacts. Whereas, with the main aim to ensure a good mechanical resistance of electrical contacts for pads, they have been filled a carbon-paste composed by 97% PDMS and 3% carbon nanotubes (CNT, purchased from Nanocyl).

A titanium wire has been put between them to be contacted with a crocodile clip. Once deposited, the PDMS-CNT paste needs to be placed in an oven approximately for one hour at a temperature of 70°C to be cured and solidified. After this treatment, the metallic wire is strongly attached to the metal and can bear mechanical stress without breaking the metallization.

From an electrical point of view, both of carbon cement paste and PDMS-CNT

paste presents similar electrical characteristics/behaviour. Indeed, both of two pastes shows an electrical resistance (in the order of tens of kΩ), leading thus to use them for electrical contacts.

To obtain the whole device, the other three PDMS layers are put one on top of the other as it can be seen in Figure 4.8; each layer is bonded one with each other thanks to a plasma-oxygen bonding process.
The characteristics of the machine are reported in section 3.1.4.

**Figure 4.8:** Assembled device

The practical way to fill chambers is through the usage of a syringe and an attached tube but since functionalization protocol involves several reagents (as deeply explained in section 4.3), every time that a liquid has to be inserted in the chamber, the syringe must be removed from the device to be filled and then attached again.

This may lead to a detachment of PDMS layers due to mechanical stress; to overcome this limit, the cubes were bonded upon the device so that the tube only stresses them and not the underlying layers that are involved in microfluidics (Figure 4.9). The hole in the cubes has a conical section to guarantee a strong connection. So, the function of this cubes is related to the maximum possible mechanical stress reduction.

It is mandatory to evaluate the absence of liquid leakages and the correct filling of both of two chambers. To perform this study, a blue dye is used to test the microfluidic, as reported in Figure 4.11.

Once established that the device was working as expected, functionalization steps were ready to be performed.

**Figure 4.9:** Particular of PDMS cubes bounded upon the device

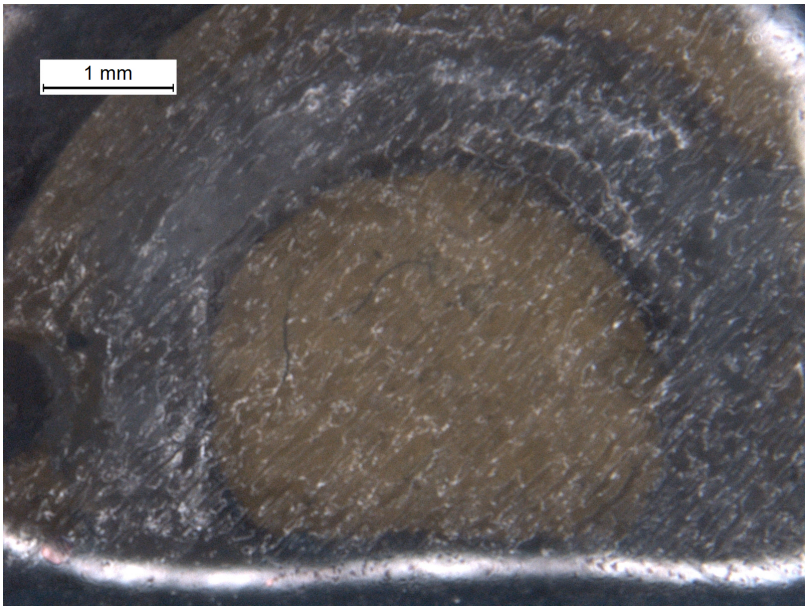


**Figure 4.10:** Picture of working electrode taken with digital microscope

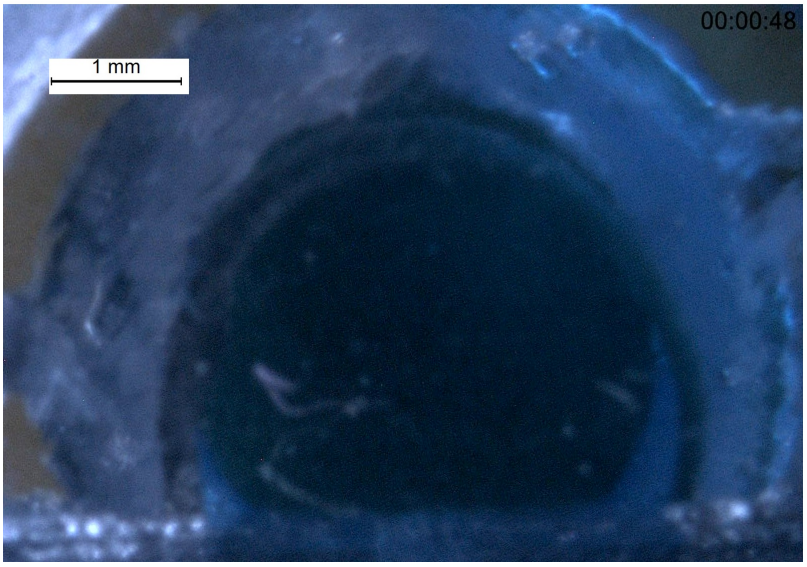


**Figure 4.11:** Picture of wet working electrode taken with digital microscope

## 4.3 Biological protocol

The first thing to be highlighted is that during the functionalization process, only the working electrode is involved; for this reason, only one channel is used, the one present in the first layer that has at the same time function of input and output.

The operations to access this channel are performed manually with a simple syringe and a tube connected to it; the value of the outer diameter of the tube must be slightly minor than the one of the inlets. This is done to ensure a proper PDMS tightening around the tube.

There are two ways of proceeding for filling the chambers, i.e. push and pull microfluidics. They are based on two opposite physical principles: when a liquid is pulled, it is attracted by a resorvoir because a depression is created inside the chamber. On the other hand, when pushing a liquid, an overpressure is originated in the chamber.

In this work, a mix of these two techniques was used: indeed, liquid was pushed into the microfluidics to fill chambers and pulled when chambers had to be emptied.

At the beginning of the process, a SAM of thiols with a COOH termination (carboxyl group) was grown on the working electrode Au surface; this is done with a solution of 3-mercapto propionic acid (3-MPA) 10 mM in a solution of ultrapure water (UPW) with the addition of 10% of ethanol (v/v) and then incubated for one hour. The concentration of ethanol has been chosen such as not to destroy the device; indeed, a too high concentration would detach the PDMS layers bonded together.

Then, the surface was washed three times with UPW.

The following step has been to incubate two different reagents for 15 minutes each: they are 2-(N-morpholino)ethanesulfonic acid (commonly known as MES) and EDC/sulfo-NHS in chronological order. EDC/sulfo-NHS (that has a composition of 4/10 mM in MES buffer at pH 5) is needed to activate the carboxyl group, whereas the function of MES is to prepare the electrode surface at the proper pH value, the same of EDC/sulfo-NHS, which in this case is equal to 5; indeed, at this value, the COOH activation reaches its maximum efficiency.

At the end, the excess of solution was washed away three times with phosphate-buffered saline (PBS). PBS is used because its pH is around 7 and this is the optimal value for protein conjugation since EDC/sulfo-NHS remains stable for a longer time.

Once arrived at this point, the antibody to be bound to the target analyte must be inserted: in this case, the target is Ang2 and so the antibody (a-Ang2) is specific for this protein. The antibody was left in contact with the underlying electrode for an entire night in a fridge at a temperature of 4°C.

Afterwards, a-Ang2 was removed and other three washes were performed, this time with PBS with an addition of 0.05% (w/v) Tween-20 (PBS-t), to perform the

washes in a more stringent manner. Last step was to add in a PBS solution the desired Ang2 concentrations and leave them in incubation for one hour; three final washes with PBS-t were carried out again.

At this point two more considerations about the device are necessary: the first one is that each device will be employed for testing different experimental conditions, i.e., with a different concentration of Ang2. Each concentration was tested in triple; this means that a specific concentration will be settled on three sensors and, therefore, the same measurement can be repeated three times.

Furthermore, once a device is functionalized (and of course after the measurement is carried out) is no longer usable. Indeed, PDMS tends to adsorb all the reagents that are employed in the protocol described above and this would heavily influence a hypothetical new functionalization [65].

After all these steps, Ang2 concentration measurements can be carried out; this will be the topic of section 4.4 whereas an explanation about the reagent involved in the operation (potassium hexacyanoferrate-II ($K_4[Fe(CN)_6]$) and potassium hexacyanoferrate-III ($K_3[Fe(CN)_6]$)) can be found in section 3.3.1.

## 4.4 Results and discussion

In this section, a focus is placed on measurements results and their interpretation. As already mentioned in section 3.3.1, a redox solution is used to perform EIS and SWV. The solution has to wet all three sensors electrodes and, for this reason, microfluidic channels that serve BC (see section 4.1) are used both to inject and to eject the fluid once the measurement is over.

Among all the possible electrochemical analytical methods, SWV and EIS were chosen to carry out the measurements presented in this work. Indeed, SWV is a widely represented and explored technique in scientific literature and one of the most successful among voltammetries [66] whereas EIS (as explained mathematically in section 3.4.1) gives the possibility to examine physical processes separately, depending on the frequency at which the measure is performed [67].

For each device, a different concentration of Ang2 was immobilized on the working electrode. As one device can host 3 sensors, 3 measurements were performed for each Ang2 concentration. The five Ang2 concentrations used in this work have been 10, 25, 50, 75 and 100 ng/mL. In addition, EIS and SWV measurements with bare electrode (i.e., without starting functionalization process), after SAM of thiols growth, and after a-Ang2 was anchored, were also performed.

In the first place, EIS was performed on each sensor. In order to do this, Palmsens device (see section 3.3.2) was configured through the software PSTrace to settle the input parameters mentioned in sections 3.4.1 and 3.4.2. Then, crocodile clips were used to contact the metallic wire present on the pads. The obtained data

were plotted on a Nyquist and a Bode plot; an example is shown in Figure 4.12 and Figure 4.13, where EIS of a sensor treated with Ang2 100 ng/mL concentration is reported.

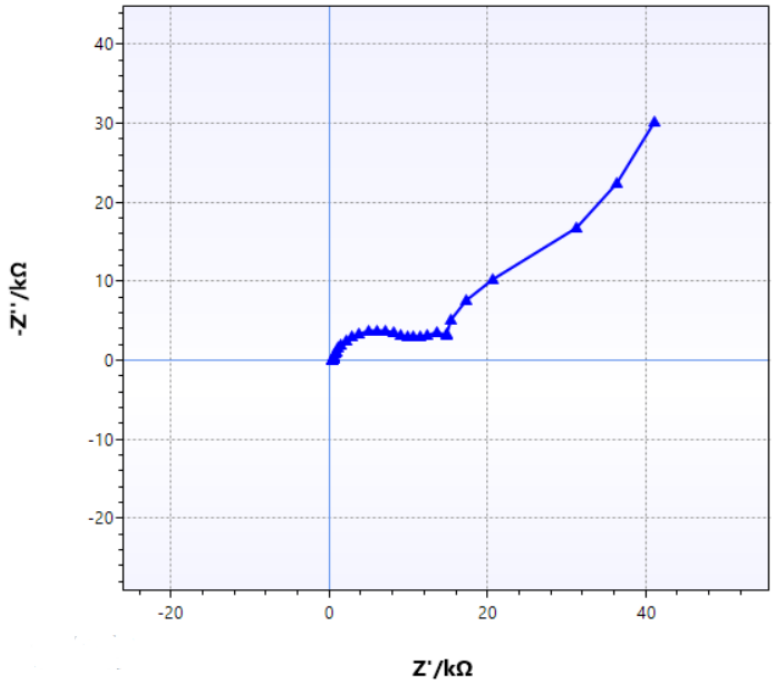


**Figure 4.12:** EIS Nyquist plot of 100 ng/mL Ang2

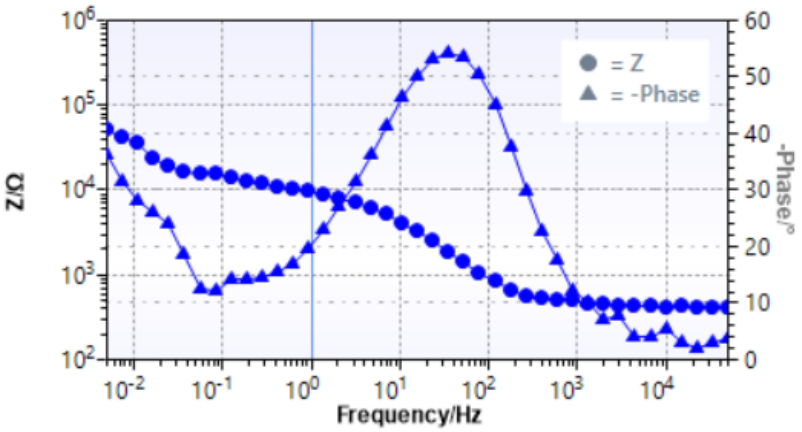


**Figure 4.13:** EIS Bode plot of 100 ng/mL Ang2

These data where fitted with software EIS Spectrum Analyzer (Figure 4.14) and values of Randles circuit elements were estimated; then, they were exported to Matlab to be processed and plotted.

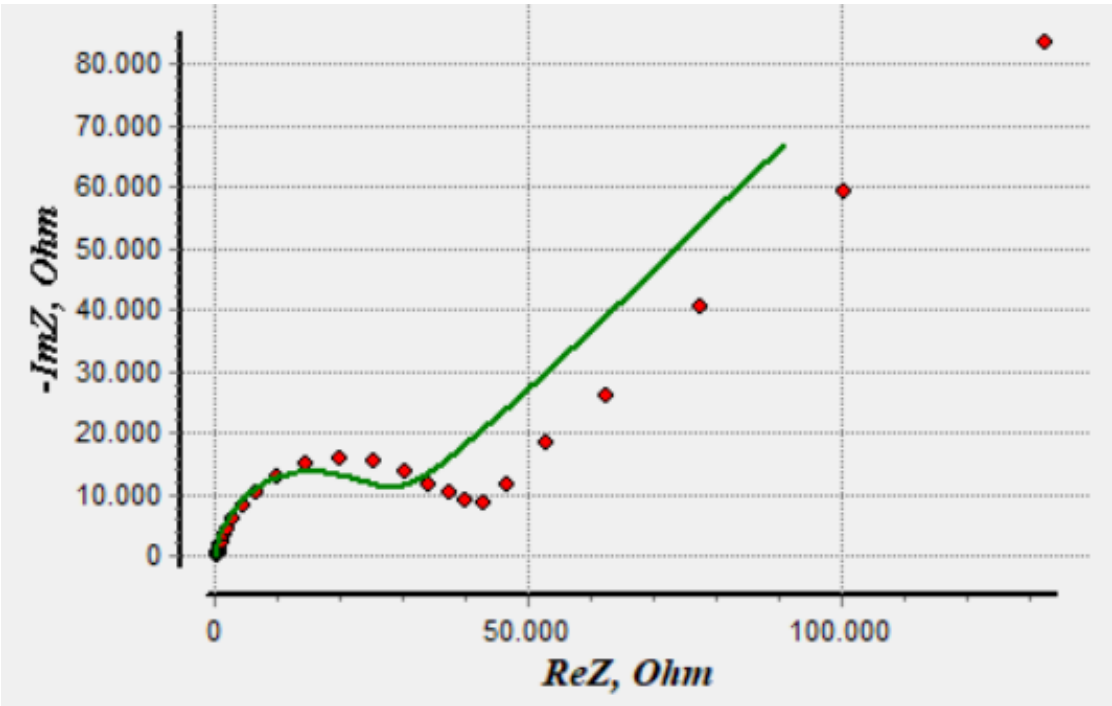


**Figure 4.14:** EIS data fitting of 50 ng/mL Ang2

### 4.4.1 Protocol monitoring

In order to check the good realization of the functionalization, EIS was performed after each step of the protocol. $R_{sol}$ and $R_{ct}$ were calculated and the results are reported in Figure 4.15 and Figure 4.16.
For what concerns $R_{sol}$, it can be seen that its value is almost constant over different steps; it was expected that this parameter did not change in different conditions since the chemical composition of the solution is always the same, independently from the species anchored to the electrodes during functionalization.
However, $R_{ct}$ presents a different behaviour; its value rises adding SAM of thiols, then it falls down when a-Ang2 is anchored and it increases again when Ang2 is detected. To explain this tendency, the isoelectric point of the proteins (i.e. a-Ang2 and Ang2) must be taken into account. The pI is the pH value at which the protein is electrically neutral. If the protein is surrounded by a solution with a pH value higher than its pI, the protein will carry positive charges; on the other hand, for a pH value lower than its pI, the total charge of the protein will be negative [68].

The pI value of a protein can be calculated using the Protein Data Bank (PDB), a worldwide database that stores information about structure of biological molecules. In the case of Ang2 the computation has been carried out on the complete amino acids sequence and the result was 5.41. The pH value of the solution used to perform electrochemical measurements (described in section 3.3.1) was measured with litmus paper and it resulted to be a value between 4 and 5.
Unfortunately, it is not possible to know a-Ang2 pI because it is an intellectual property of the company that owns it but, on the basis of the data in Figure 4.16, a hypothesis can be formulated, i.e. that a-Ang2 pI values is below solution pH value.

This would explain in a coherent way $R_{ct}$ behaviour: a-Ang2 immersed in the measurement solution presents a positive surface charge, facilitating electrons movement and, therefore, leading to a decrease of $R_{ct}$. On the contrary, with the addition of Ang2, protein surface charge is reversed and it becomes negative, hindering electrons transfer [68].

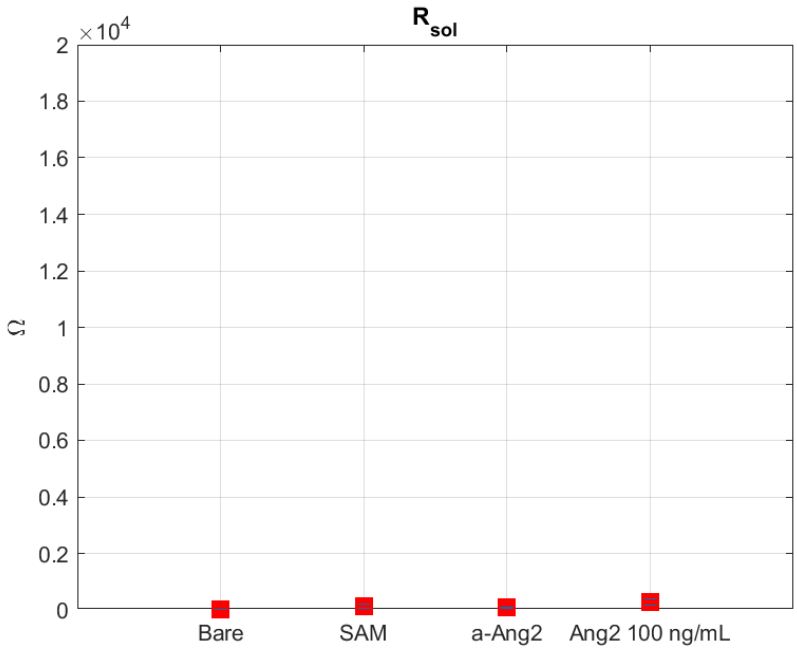


**Figure 4.15:** Solution resistance evaluation

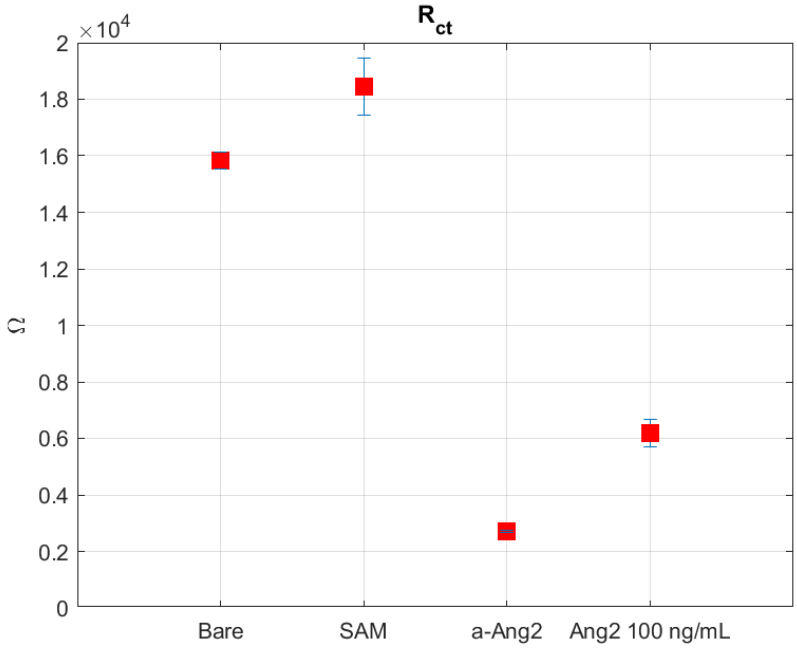


**Figure 4.16:** Charge transfer resistance evaluation

### 4.4.2 Ang2 detection

After this first step, the following measurements involved the different Ang2 concentrations already mentioned; the results are shown in Figure 4.17 together with Randles circuit used as model.

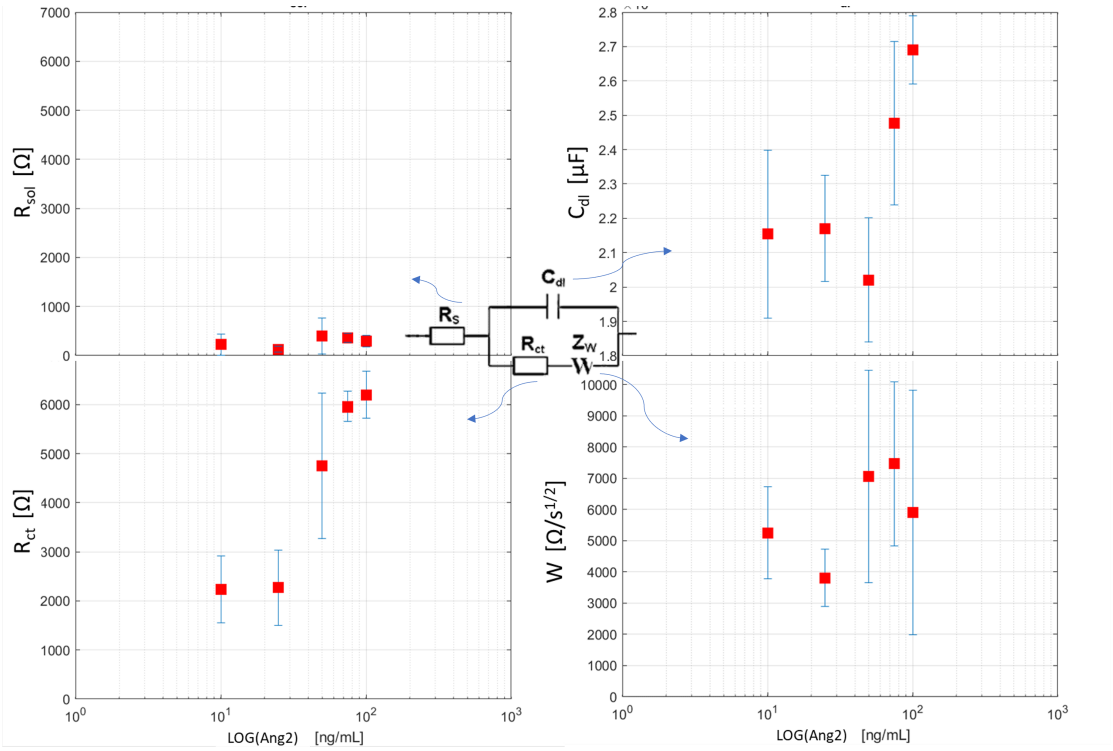


**Figure 4.17:** Randles circuit and relative electrical circuit parameters measurements

As it was done in the first measurements, $R_{sol}$ has been calculated to check that the solution was not changing over time and this is guaranteed from its constant trend.

Focusing on $R_{ct}$, it is possible to see that its value seems to be independent from Ang2 concentration for 10 and 25 ng/mL. Starting from 50 ng/mL, it starts to grow as Ang2 concentration also increases. This result was expected since with a higher Ang2 concentration, the electrons present in the solution found more obstacles to reach metal electrode surface, leading to an increase of $R_{ct}$.

Looking at $C_{dl}$, considerations similar to the ones related to $R_{ct}$ can be made: indeed, capacitance is expected to slightly increase with Ang2 concentration [68].

Finally, analysing $Z_W$ results, it can be seen that diffusion data are not particularly significant since it is difficult to distinguish a clear trend. Our hypothesis

for this absence of a clear trend in the diffusion is that the PDMS barrier used to separate SC and BC may hinder diffusion process.

Nevertheless, the benefits obtained from SC and BC (the fact that functionalization and measurements steps can be completely separated and handled independently) are good enough to overcome the limitation in $Z_W$ evaluation; for this reason, it was decided to focus the attention on the most clear and significant parameter, i.e. $R_{ct}$.

Besides this, two additional graphs regarding $R_{ct}$ and $C_{dl}$ are shown in Figure 4.18 and 4.19. In this case, a normalization of these two values (for different Ang2 concentrations) with respect to charge transfer resistance and double layer capacitance after a-Ang2 anchoring ($R_0$ and $C_0$) was plotted; this graph is useful to calculate different sensitivities (in this case referred to $R_{ct}$ and $C_{dl}$) and to compare them.

Indeed, evaluating the slope of the line that fits best (in the sense of least-squares method) the data sets in figure, $R_{ct}$ and $C_{dl}$ sensitivities can be computed. In this case they have respectively a value of 1.5573 and 0.3885. From this plot it can also be stated that the device seems to be insensitive to low Ang2 concentrations such as 10 and 25 ng/mL (and also to 50 ng/mL in the case of $C_{dl}$).

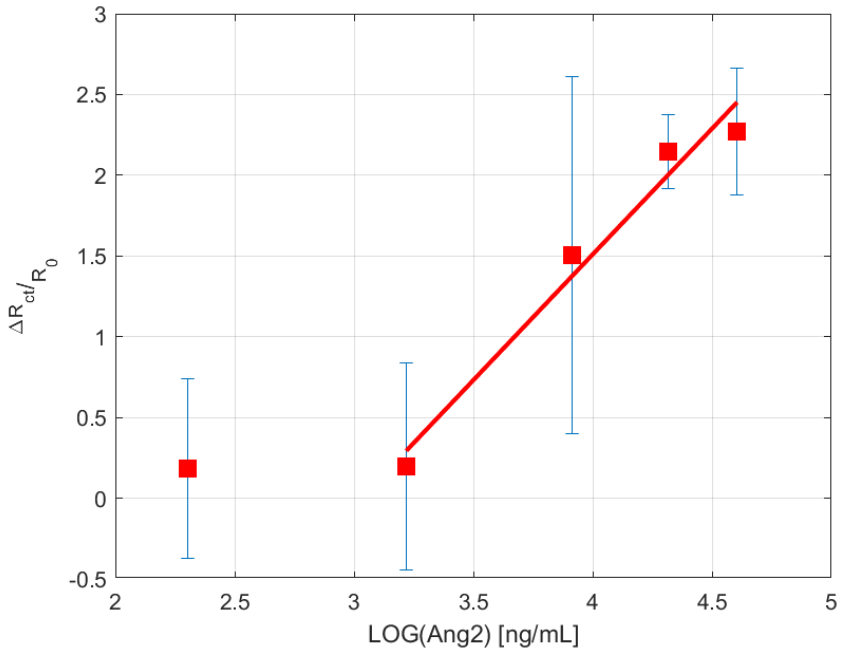


**Figure 4.18:** Electrochemical characterization of the sensor in terms of $R_{ct}$

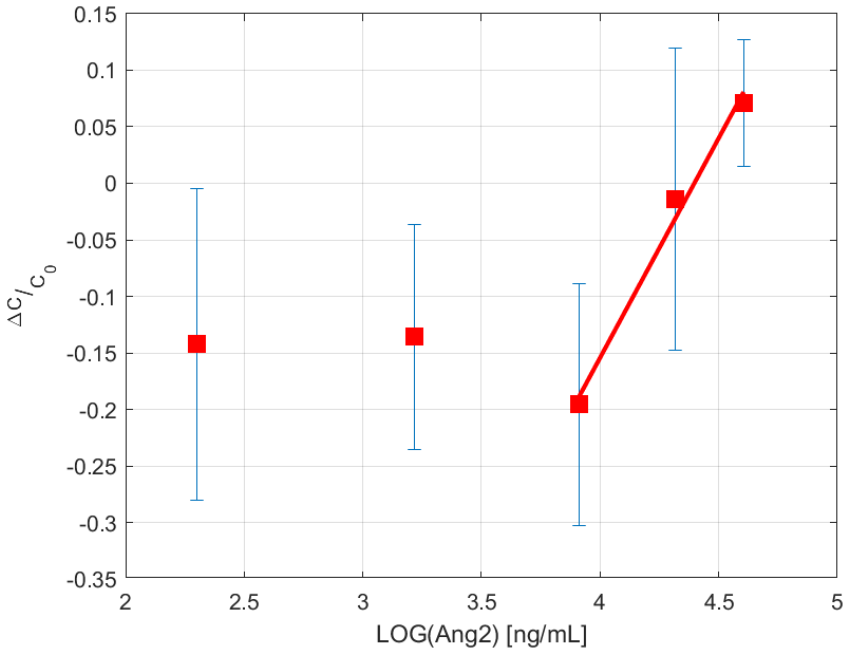


**Figure 4.19:** Electrochemical characterization of the sensor in terms of $C_{dl}$

After the analysis of EIS results, SWV measurements were taken into account: a graph with peak current value trend with respect to Ang2 concentration is reported in Figure 4.20.

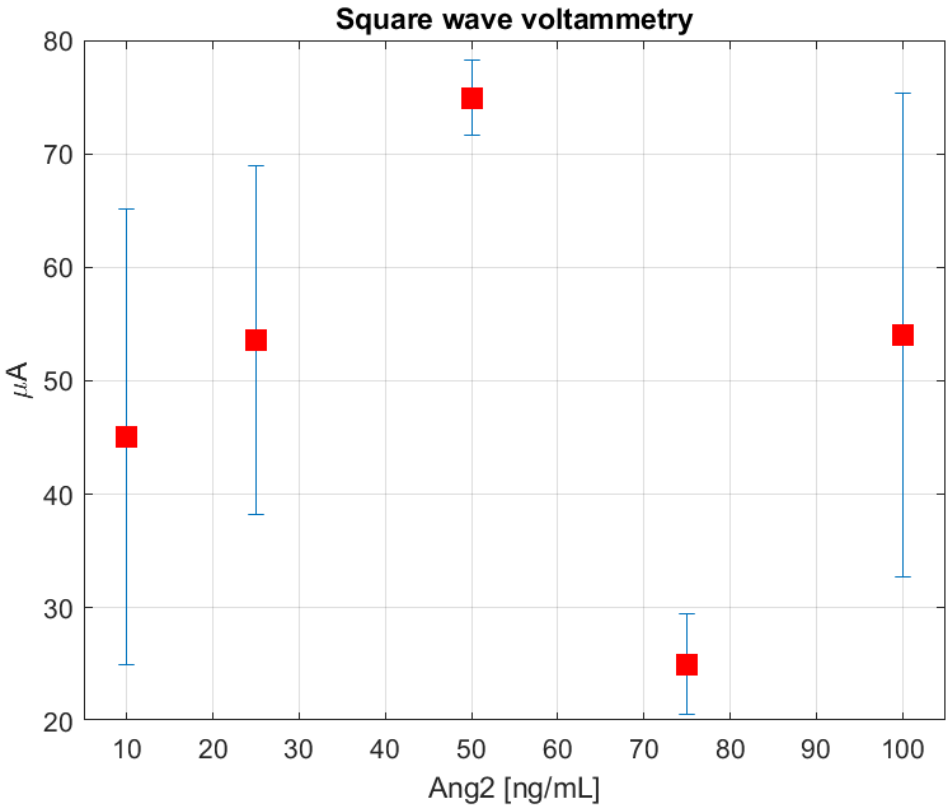


**Figure 4.20:** Peak current evaluation

In this case, results are not as satisfactory as EIS ones; indeed, since there is an increase of $R_{ct}$ with the increment of Ang2 concentration, a decrease of peak current value would be expected. This is not the case since it seems that current value is independent from Ang2 concentration.

The explanation is related to the number of physical processes that happen simultaneously: indeed, whereas EIS allows to separate different processes (and their effects) depending on the applied frequency, when performing SWV all the processes cannot be distinguished from one to another and a superposition of all their effects is present.

For this reason, the focus was placed on EIS such that a good uncoupling of which process is prevailing in every moment is always possible thanks to the electrical circuit model. Furthermore, this was precisely the goal of this setup

phase: to understand which electrochemical technique was the most suitable for this kind of device.

Finally, once collected and analysed all the data, some improvements for device structure were conceived: first of all, a larger amount of measurements is desirable in order to guarantee a higher system throughput. But the more important feature to be integrated in the device would be the possibility to carry on multiplexed and real time measurements in order to increase the device versatility and to make it more user friendly, reducing the interaction needed with the final user.

To accomplish these goals, a new device design was developed; chapter 5 is dedicated to its description.

# Chapter 5

# Second device design and optimization

The aim of this work has been to build a reliable and low cost system in which up to three sensors can be functionalized at the same time. Once established that the device (and the microfluidic integrated in it) properly accomplish to their function, the following step is to automatize more the system, to make it more efficient and to allow multiplexed real time measurements.

Up to now, the device has been entirely built in PDMS (except for the metallizations) and this makes it disposable since it tends to absorb reagents used in functionalization; indeed, the steps described in section 4.3 are mandatory and they can not be avoided. On the other hand, many measurements (instead of a single one) could be in principle performed on the same sensor, even over time, if PDMS structure would be removed. For this reason, a different paradigm has been adopted; the whole system is no more a single device but it is composed by three different units, i.e. a common basis to host sensors and two caps, one used for functionalization (Functionalization Cap, FC) and the other for measurements (Measurements Cap, MC).

The biggest difference with respect to the device described in chapter 4 is that the basis, FC and MC are not meant to be employed all together at the same time; obviously, the basis will always be present but caps will be used one at a time, depending on whether functionalization or measurements operations must be performed.

This implies that the device will be manipulated even after its building to substitute caps (in particular FC will be substituted by MC since functionalizaton is always done as first step) but then it may be used for a longer time because more measurements could be performed once MC is assembled on top of the basis.

FC and MC present several differences that will be exposed and explained along

this chapter but the more evident one is the material they are constructed with. FC will be made by PDMS since it is a low cost and biocompatible solution for a device component that will be used only once; MC, alongside with the basis, will be manufactured with a plastic material that would guarantee a longer usage.

The complexity of this device is quite high and it was not possible nor affordable to use 2D models produced with laser ablation machine; instead, more complex 3D models were designed with Rhinoceros CAD with the objective to export them in a suitable format for a 3D printing machine.

One of the limitations that can be overcome thanks to this choice are the device dimensions so that more than three sensors can be hosted: this can allow to work with more analyte concentrations at the same time (since each concentration can be used on a different triple) or, alternatively, more measurements with the same concentrations can be carried out. This last case can be particularly useful in the validation phase of the technology, since lots of data to verify device functionality are needed.

For the reasons explained above, device basis design has been deeply revised with respect to the version shown in section 4.2. The new conceived design is shown in Figure 5.1 and Figure 5.2.

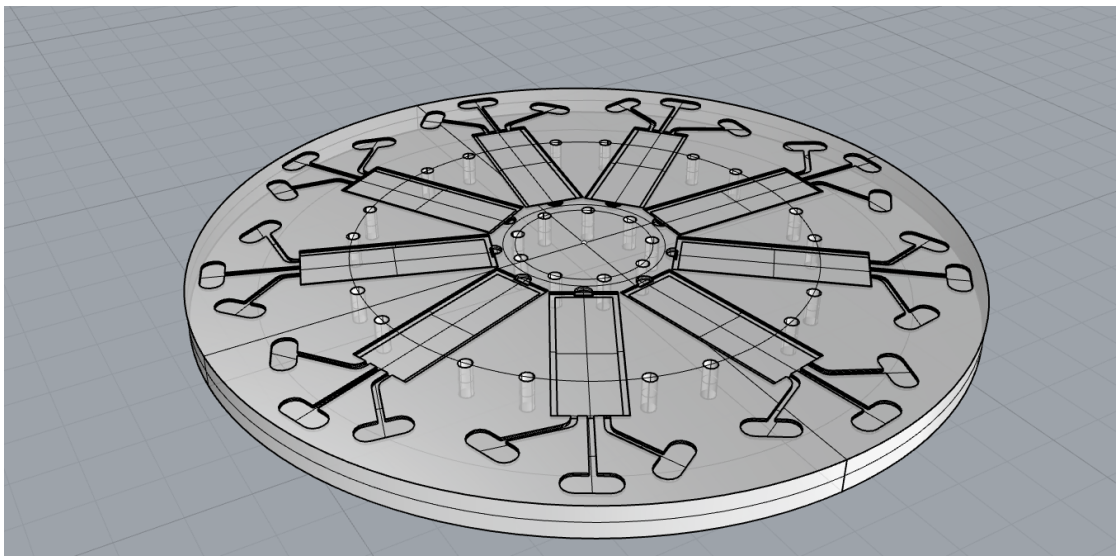

**Figure 5.1:** 3D device basis

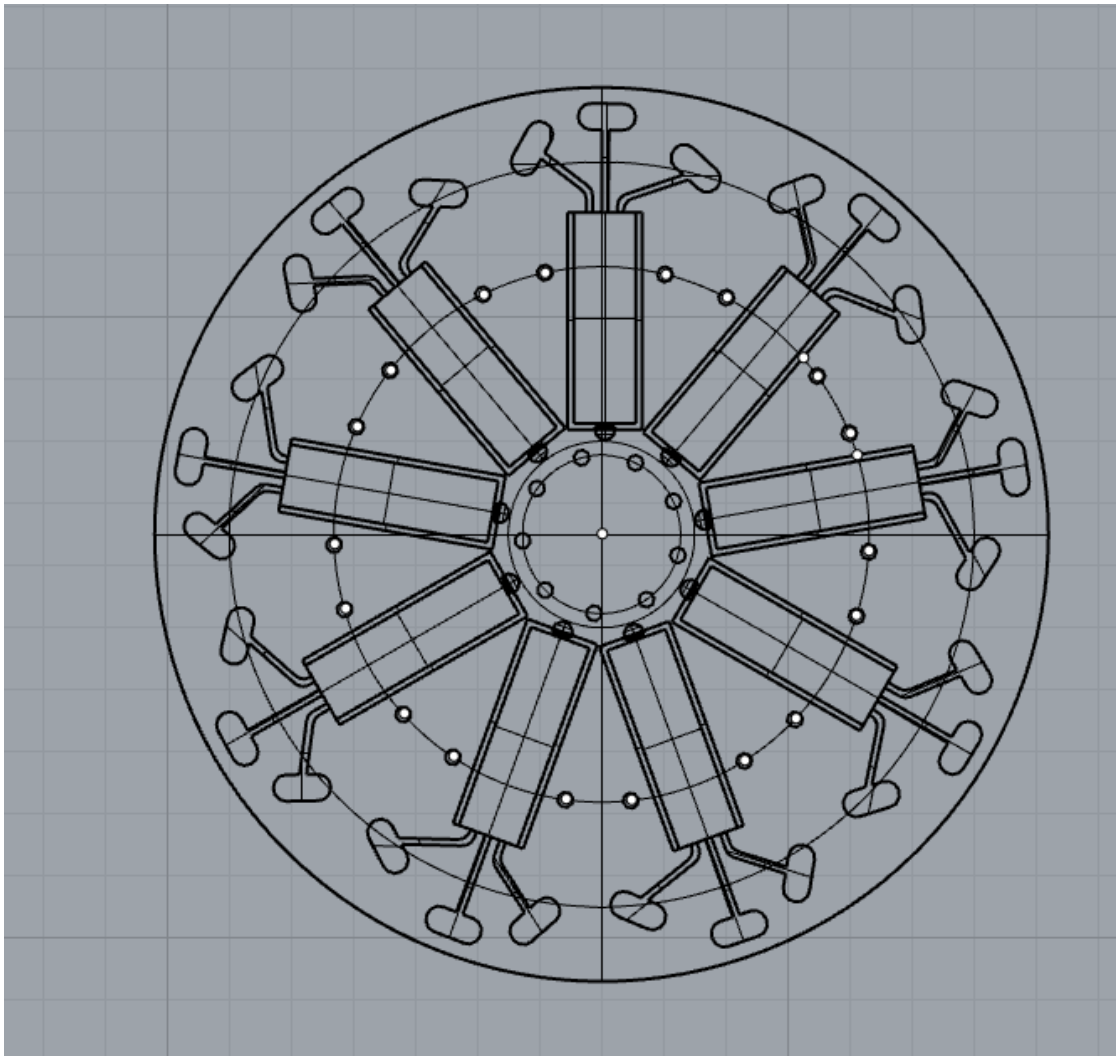

**Figure 5.2:** 3D device basis top view

The new structure is a cylinder with a height of 0.6 cm and a diameter of 14.4 cm: this allows to have a working surface which is more than three times bigger with respect to the one that can be obtained with laser ablation machine. In this way, nine sensors (i.e. three triples) can be hosted. At the same time, the basis is thick and lightweight enough to be manipulated and transported by hand with no particular effort.

Sensor slots, paths and pads have the same dimension and function of those already introduced and explained in section 4.1; paths have all the same length in order to make the metallization resistance approximately the same. Among new design features, a small cavity (shown in Figure 5.3) has been added on top of the slots to facilitate sensors extraction with a pair of tweezers.
Furthermore, several through holes (with a diameter of 0.25 cm) are present in order to attach basis and caps with screws; in this device there is no plasma bonding and the assembly is completely mechanical. As it can be seen in Figure 5.4 and Figure 5.5, there are nine holes in the device centre and two holes between each two sensor slots for a total of 27 screws.

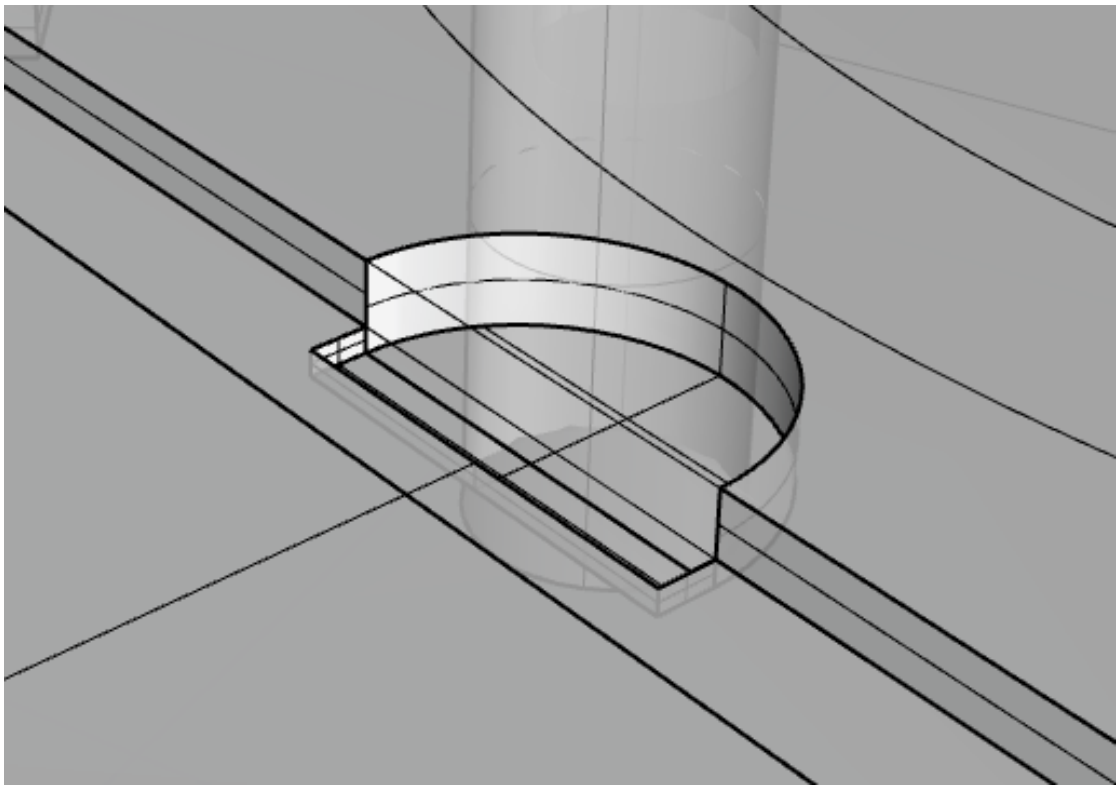

**Figure 5.3:** Cavity to manually extract sensors

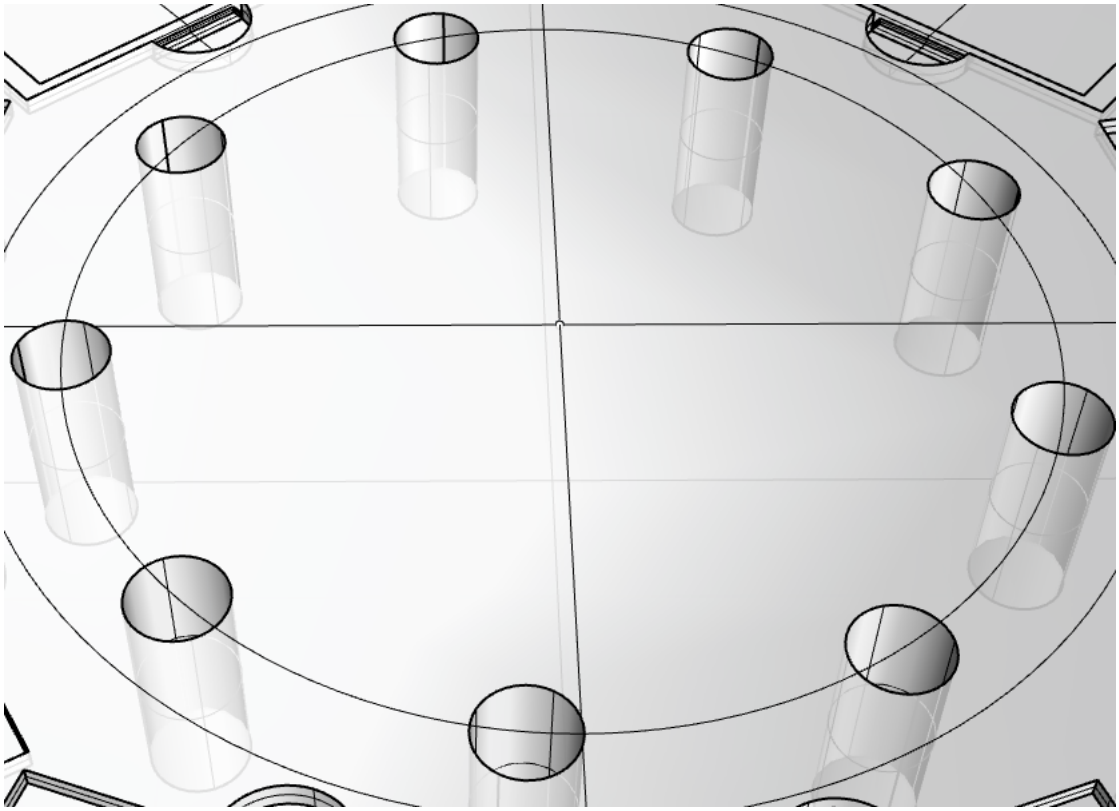

**Figure 5.4:** Centre device holes

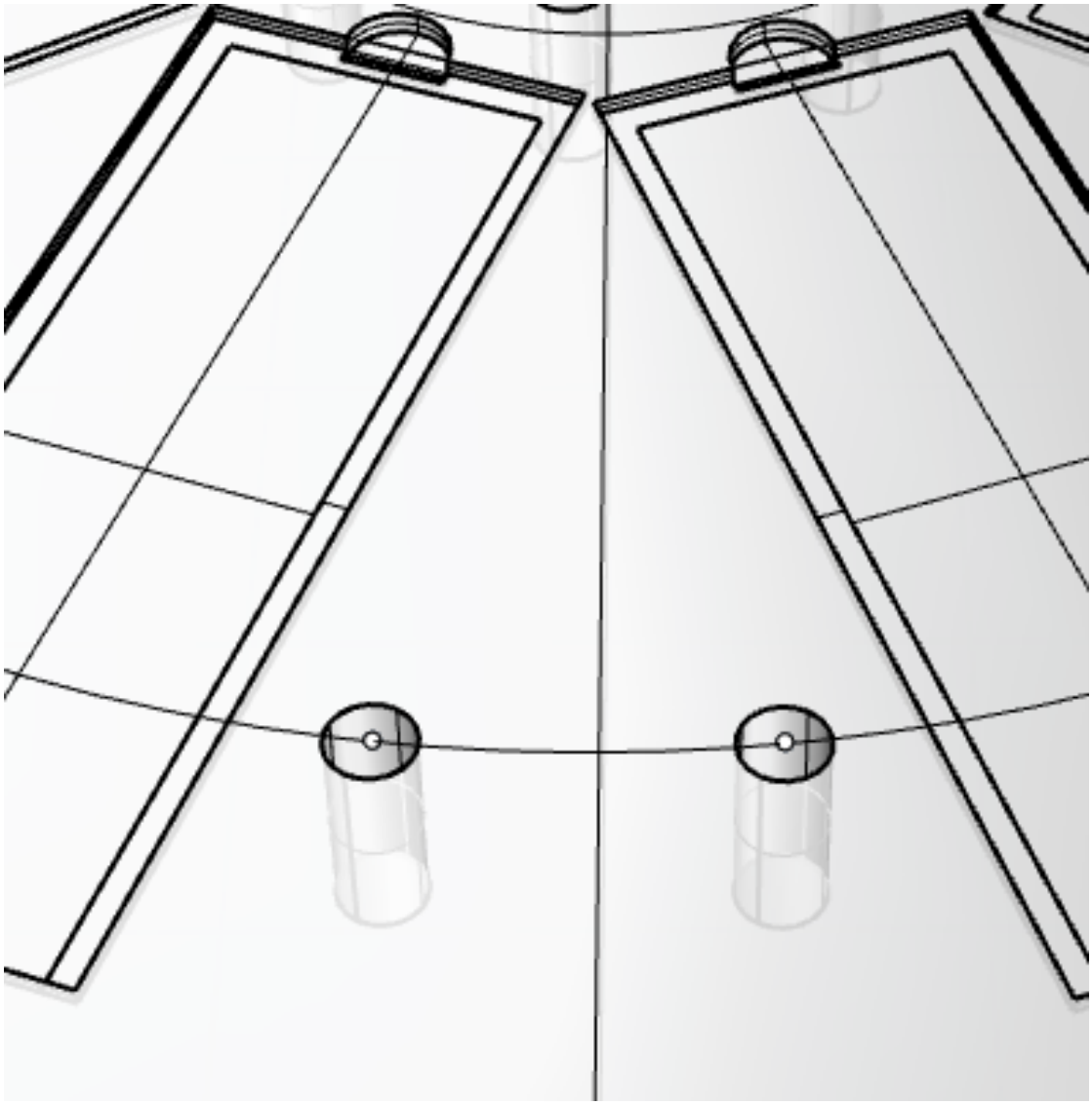

**Figure 5.5:** Through holes between two sensor slots

Also caps design is conceptually very different with respect to the PDMS layers seen in section 4.2; yet, except for the material they are made with and for the microfluidics, FC and MC are quite similar; therefore they will be discussed together, highlighting the differences between them from time to time.

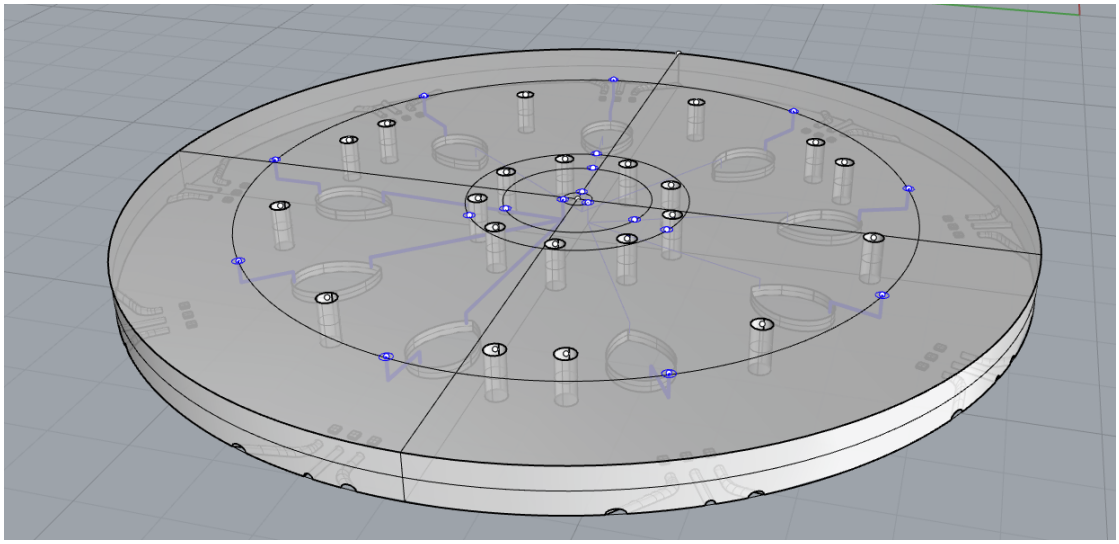

**Figure 5.6:** Functionalization cap

First of all, both caps dimensions are reduced with respect to basis: they have a height of 0.57 cm and a diameter of 11.4 cm. This is due to the fact that pads, that are located almost on the border of the circle, must be reached from outside world to provide electrical signal and they cannot be covered by any cap.

As it can be seen in Figure 5.7 tunnels are dug in correspondence of the metallic paths of each sensor; this is done to prevent possible scratches or damages on metallization that may be caused by the cap.

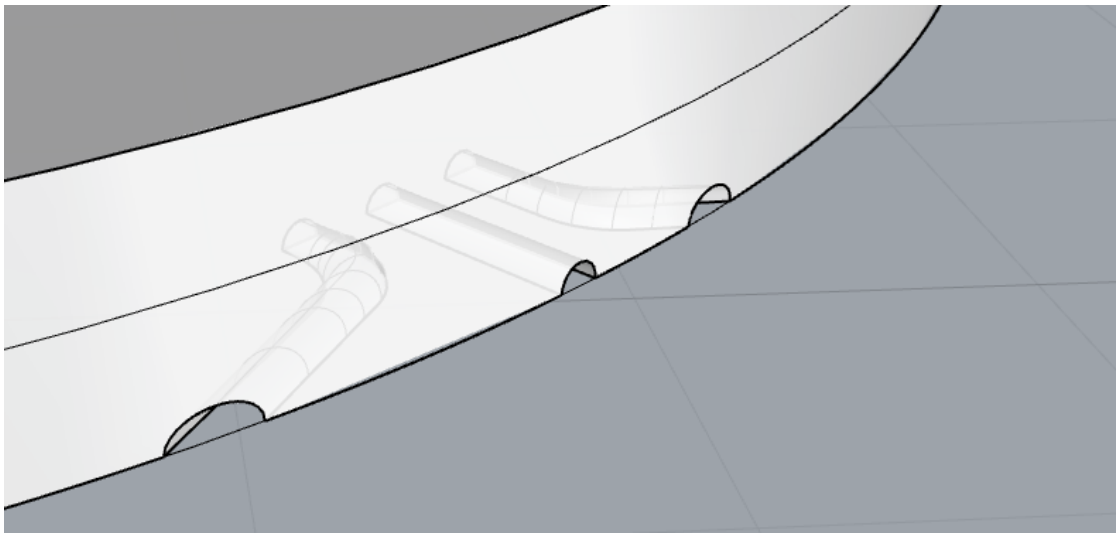

**Figure 5.7:** Tunnels dug in FC

In addition to the tunnels, MC is equipped with another feature that is worth to be discussed; a clearer view from down side is given in Figure 5.8.

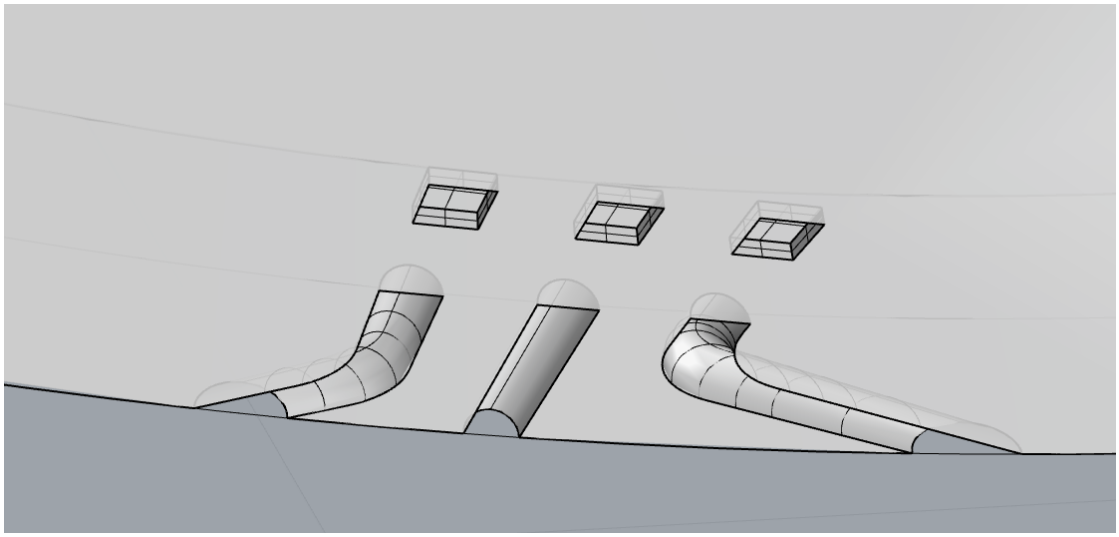

**Figure 5.8:** Detail of tunnels and metallic "bridge" of MC seen from below

The squares shown above are placed in correspondence of the interface between metallic paths and sensor metal stripes and they have the same function of the metallic bridge in the PDMS-built device: indeed, they are used to guarantee electrical continuity between sensor and metallic paths since it would be impossible to deposit a metallic line as thick as the sensor. The idea is to reverse upside down MC and to fill it with metal using screen printing technique; then, it would be again reversed to be placed in contact with the basis. Also metal in paths and pads can be deposited by screen printing with the same materials described in section 4.2: carbon cement for the paths and a mix of carbon cement and PDMS-CNT paste for the pads.

Another difference with respect to PDMS-built device is represented by the chamber where functionalization and measurements take place; In this case, instead of a double concentric structure, the chamber is droplet-shaped in order to facilitate the wetting of the electrodes; furthermore, area and volume have been calculated to be able to host a sufficient reagents volume inside the chambers. More specifically, they can be filled with approximately 90 $\mu$L. In Figur 5.9 and Figure 5.10, views of a chamber in section and seen from below can be appreciated.

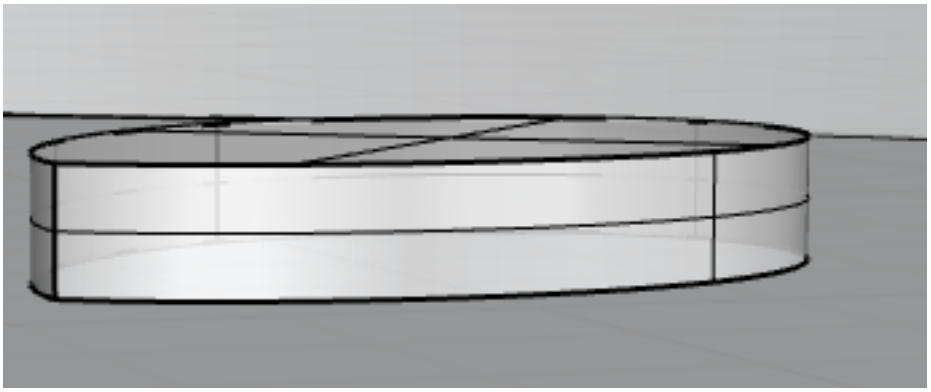

**Figure 5.9:** Chamber seen in section

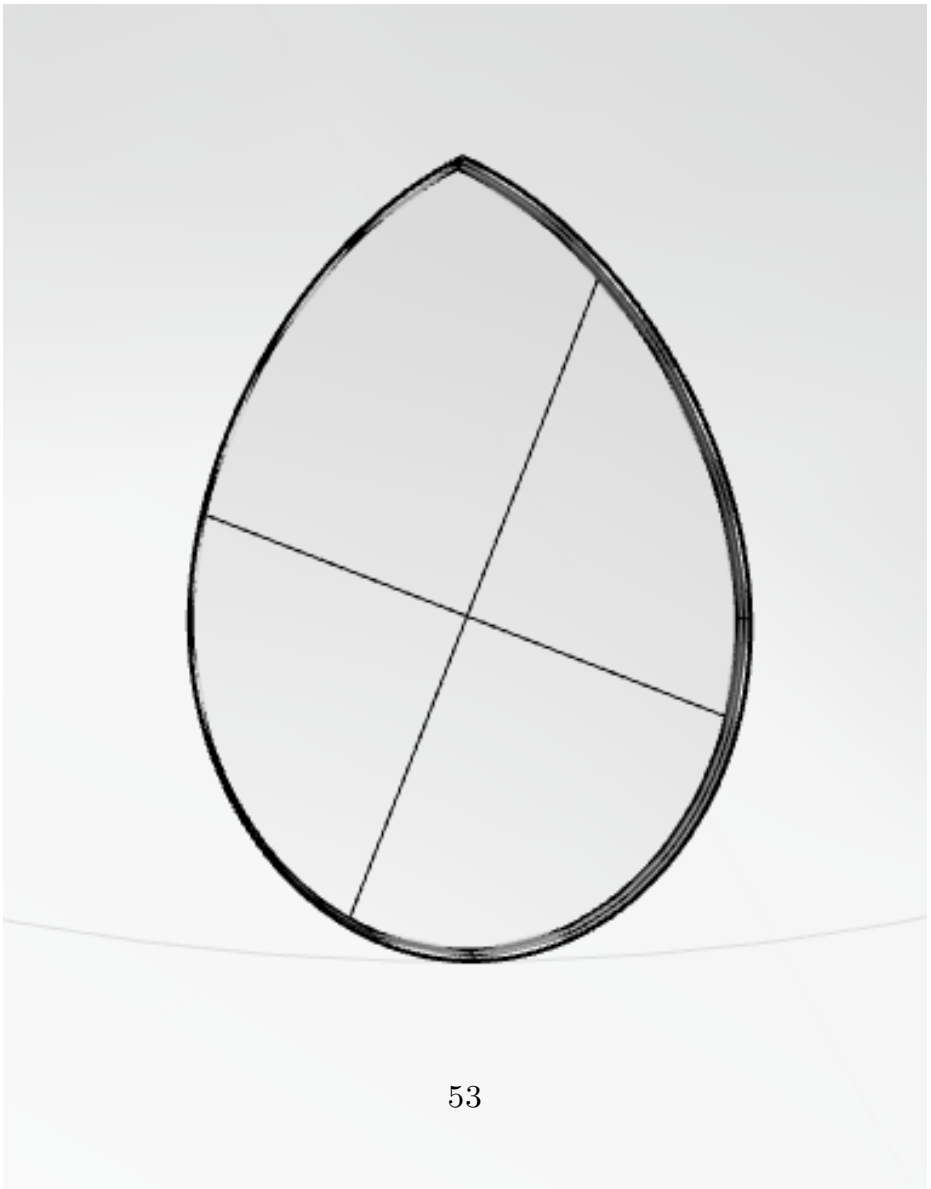



**Figure 5.10:** Chamber seen from below

Finally, the most important novelty in the device design is related to the microfluidics since it brings new functionalities and improvements: the most significant one is the increasing velocity in measurements. To better explain this concept, it is useful to see a top view of one of the two caps (MC in this case) that is shown in Figure 5.11.

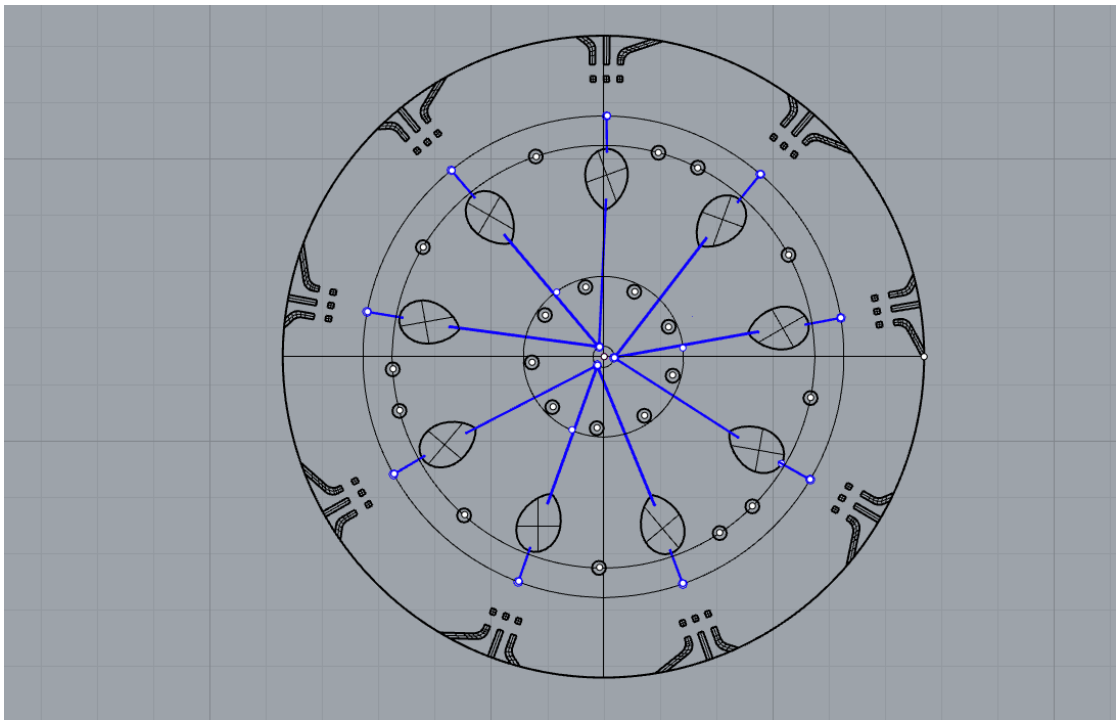

**Figure 5.11:** MC top view

It can be seen that there are three inlets placed at a very small distance from the cap centre and nine external outlets, close to cap borders. Each inlet serves three sensors (a triple) and each sensor is coupled with its own outlet. This means that every reagent that is inserted into an inlet can reach simultaneously three sensors; thus, up to three measurements in the same experimental conditions (i.e., same biomarker concentration) can be carried out, overcoming limitations present in the PDMS-built device. This concept can be widely stressed by inserting in every inlet different biomarker concentrations or even different target analytes, since each triple is independent from the others. In conclusion, up to nine concurrently measurements can be performed, leading to rapid results that, when cancer is involved, can be decisive to save a patient's life. On the contrary, there is one outlet for each sensor: reagents exiting from the chambers are usually trashed but sometimes they could be analysed (for example, their pH may be measured) for better troubleshooting possible problems highlighted by results.

It is also interesting to look at the caps in section to see how microfluidic channels are designed; since they will be built with 3D printing machines (used as moulds for PDMS in FC or directly as cap in MC), the channels do not need to lay on a plane but they also have a vertical dimension. In Figure 5.12 channels belonging to FC are shown.

These channels have a square section (with a diagonal of 250 $\mu$m) and they only present right angles; this choice has be taken in order to better extract PDMS cap from its mould.

In Figure 5.13 MC microfluidic channels are shown in section.

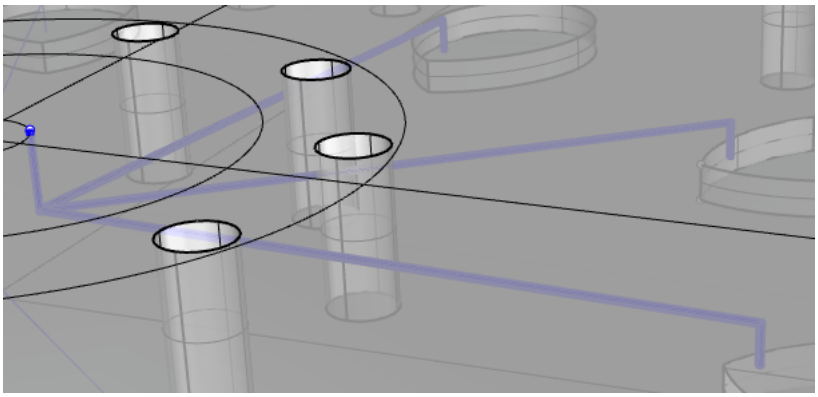

**Figure 5.12:** Microfluidic channels in functionalization cap

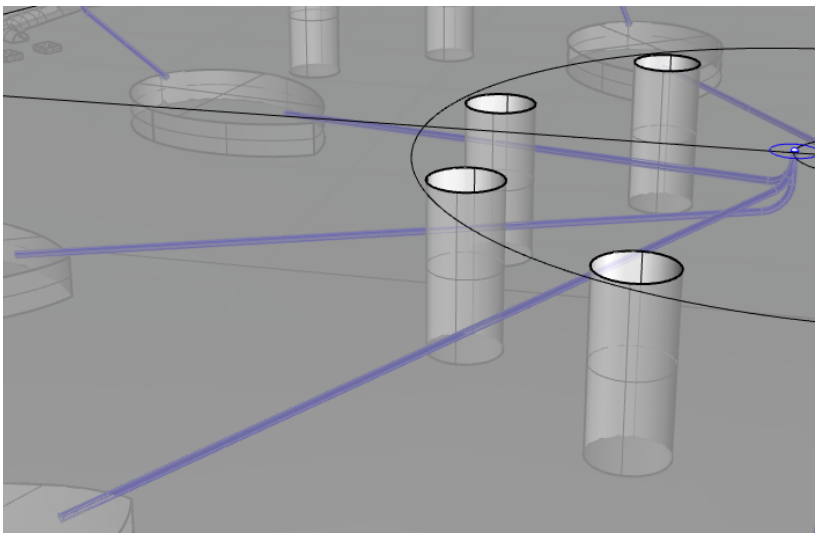

**Figure 5.13:** Microfluidic channels in measurement cap

In this case, their section is circular with a diameter of 250 $\mu$m and they present rounded corners; this is because MC is thought to be directly built with a 3D printer and these machines use sacrificial layers to sustain mechanically the structure during the construction. At the end, these layers have to be removed and it is easier to do it in absence of sharp edges.

In conclusion, this design can provide a higher throughput, since there is the possibility to carry out many measurements in parallel, and a more versatile device that the final user can adapt in several different ways simply choosing which triples have to be used and which biomarkers have to be inserted in. In this way, measurements are really multiplexed, providing a huge degree of freedom when an experiment is set up. The device is also thought to be long-lasting in time, since MC can be used many times; this leads to a reduction in PDMS consumption and to a more user friendly device because if the same measurement has to be repeated many times, functionalization steps have to be performed only the first time.

# Chapter 6

# Conclusions and perspectives

The aim of this work was to design and build a microfluidic-based device for electrochemical biosensing of Ang2, a specific biomarker for lung cancer.

PDMS was chosen as building material because it allowed the development of a biocompatible device, useful also for troubleshooting due to its transparency. In addition, no cleanroom technologies were used to produce the platform, leading to a cheaper alternative with respect to most of the devices available on the market.

From a microfluidic point of view, thanks to the double concentric chambers structure, it was possible to completely separate functionalization and measurements processes; indeed, each set of microfluidic channels served the two chambers independently.

Furthermore, the employment of microfluidics has allowed to easily perform the sample preparation and the analyte detection on the same platform, ensuring a simplification in the usage of the device.

After that, the surface of the sensors was functionalized by means of a SAM layer and electrochemical measurements were carried out using two different methods: EIS and SWV.

The goal was to find the best technique to successfully detect Ang2. The devices were tested with different analyte concentrations. Experimental results have shown that the data obtained with EIS, fitted and modelled with Randles circuit, are a more significant indicator of Ang2 detection; in particular, the most representative parameter has been identified in the charge transfer resistance.

Once tested the device, a new design was conceived to create a multiplex sensing platform, in particular to increase the number of measurements that can be performed at the same time. Furthermore, this new version gives the possibility to build a non-disposable device on which multiplexed and real-time measurements

can be performed. This would allow to significantly reduce the interaction with the user, since all the reagents may be prepared in advance and provided to the device with the aid of an automatized system, like a peristaltic pump. Moreover, different analyte concentrations (and even different target analytes) may be employed at the same time on the device.

Therefore, this will be the future perspective of this work: to verify the new device functionalities by building and testing it. These new characteristics may provide a faster and more reliable detection of biomarkers, that would lead to a more effective disease screening and, possibly, to a more accurate diagnosis.

# Bibliography


[1] Jacques Ferlay, Murielle Colombet, Isabelle Soerjomataram, Donald M Parkin, Marion Piñeros, Ariana Znaor, and Freddie Bray. «Cancer statistics for the year 2020: An overview». In: *International Journal of Cancer* (2021) (cit. on p. 1).

[2] Richard R Love, Howard Leventhal, Douglas V Easterling, and David R Nerenz. «Side effects and emotional distress during cancer chemotherapy». In: *Cancer* 63.3 (1989), pp. 604–612 (cit. on p. 1).

[3] JJ Ott, A Ullrich, and AB Miller. «The importance of early symptom recognition in the context of early detection and cancer survival». In: *European Journal of Cancer* 45.16 (2009), pp. 2743–2748 (cit. on p. 1).

[4] Klaus Wandelt. *Encyclopedia of interfacial chemistry: surface science and electrochemistry*. Elsevier, 2018 (cit. on p. 3).

[5] Avraham Rasooly and James Jacobson. «Development of biosensors for cancer clinical testing». In: *Biosensors and Bioelectronics* 21.10 (2006), pp. 1851–1858 (cit. on p. 3).

[6] George Luka et al. «Microfluidics integrated biosensors: A leading technology towards lab-on-a-chip and sensing applications». In: *Sensors* 15.12 (2015), pp. 30011–30031 (cit. on pp. 3, 4, 11).

[7] Kyung-Ho Lee and Dong-Myung Kim. «In vitro use of cellular synthetic machinery for biosensing applications». In: *Frontiers in pharmacology* 10 (2019), p. 1166 (cit. on p. 3).

[8] Sunil Mittal, Hardeep Kaur, Nandini Gautam, and Anil K Mantha. «Biosensors for breast cancer diagnosis: A review of bioreceptors, biotransducers and signal amplification strategies». In: *Biosensors and Bioelectronics* 88 (2017), pp. 217–231 (cit. on p. 3).

[9] Kathryn L Brogan and David R Walt. «Optical fiber-based sensors: application to chemical biology». In: *Current Opinion in Chemical Biology* 9.5 (2005), pp. 494–500 (cit. on p. 3).

[10] Gary L Long and James D Winefordner. «Limit of detection. A closer look at the IUPAC definition». In: *Analytical chemistry* 55.7 (1983), 712A–724A (cit. on p. 3).

[11] Mar Alvarez and Laura M Lechuga. «Microcantilever-based platforms as biosensing tools». In: *Analyst* 135.5 (2010), pp. 827–836 (cit. on p. 3).

[12] Jan Rickert, Andreas Brecht, and Wolfgang Göpel. «Quartz crystal microbalances for quantitative biosensing and characterizing protein multilayers». In: *Biosensors and Bioelectronics* 12.7 (1997), pp. 567–575 (cit. on p. 3).

[13] Ralf Lucklum and Peter Hauptmann. «Acoustic microsensors—the challenge behind microgravimetry». In: *Analytical and bioanalytical chemistry* 384.3 (2006), pp. 667–682 (cit. on p. 3).

[14] Fraser A Armstrong, H Allen O Hill, and Nicholas J Walton. «Direct electrochemistry of redox proteins». In: *Accounts of Chemical Research* 21.11 (1988), pp. 407–413 (cit. on p. 4).

[15] Todd P Silverstein. «Oxidation and reduction: Too many definitions?» In: *Journal of Chemical Education* 88.3 (2011), pp. 279–281 (cit. on p. 4).

[16] HL Kies. «Coulometry». In: *Journal of Electroanalytical Chemistry (1959)* 4.5 (1962), pp. 257–286 (cit. on p. 4).

[17] Eric Bakker and Ernö Pretsch. «Modern potentiometry». In: *Angewandte Chemie International Edition* 46.30 (2007), pp. 5660–5668 (cit. on p. 4).

[18] Patricia Batista Deroco, Juliana de Fátima Giarola, Dagwin Wachholz Júnior, Gustavo Arantes Lorga, and Lauro Tatsuo Kubota. «based electrochemical sensing devices». In: *Comprehensive Analytical Chemistry*. Vol. 89. Elsevier, 2020, pp. 91–137 (cit. on p. 4).

[19] Richard S Nicholson. «Theory and application of cyclic voltammetry for measurement of electrode reaction kinetics.» In: *Analytical chemistry* 37.11 (1965), pp. 1351–1355 (cit. on p. 4).

[20] Nasrullah Shah, Muhammad Balal Arain, and Mustafa Soylak. «Historical background: milestones in the field of development of analytical instrumentation». In: *New Generation Green Solvents for Separation and Preconcentration of Organic and Inorganic Species*. Elsevier, 2020, pp. 45–73 (cit. on p. 4).

[21] Aziz Amine and Hasna Mohammadi. «Amperometry». In: *Ref. Modul. Chem. Mol. Sci. Chem. Eng* (2018) (cit. on p. 5).

[22] Jian-Guo Guan, Yu-Qing Miao, and Qing-Jie Zhang. «Impedimetric biosensors». In: *Journal of bioscience and bioengineering* 97.4 (2004), pp. 219–226 (cit. on p. 5).

[23] Kihak Gwon, Seonhwa Lee, Hakhyun Nam, and Jae Ho Shin. «Disposable strip-type biosensors for amperometric determination of galactose». In: *Journal of Electrochemical Science and Technology* 11.3 (2020), pp. 310–317 (cit. on p. 5).

[24] Jung A Lee, Seongpil Hwang, Juhyoun Kwak, Se Il Park, Seung S Lee, and Kwang-Cheol Lee. «An electrochemical impedance biosensor with aptamer-modified pyrolyzed carbon electrode for label-free protein detection». In: *Sensors and Actuators B: Chemical* 129.1 (2008), pp. 372–379 (cit. on p. 5).

[25] Nelson AF Silva, Manuel J Matos, Amin Karmali, and Maria M Rocha. «An electrochemical biosensor for acrylamide determination: merits and limitations». In: *Portugaliae Electrochimica Acta* 29.5 (2011), pp. 361–373 (cit. on p. 5).

[26] Andreas Weltin, Jochen Kieninger, Barbara Enderle, Anne-Kathrin Gellner, Brita Fritsch, and Gerald A Urban. «Polymer-based, flexible glutamate and lactate microsensors for in vivo applications». In: *Biosensors and Bioelectronics* 61 (2014), pp. 192–199 (cit. on p. 5).

[27] Patrick Tabeling. *Introduction to microfluidics*. OUP Oxford, 2005 (cit. on p. 8).

[28] Jack W Judy. «Microelectromechanical systems (MEMS): fabrication, design and applications». In: *Smart materials and Structures* 10.6 (2001), p. 1115 (cit. on p. 8).

[29] George M Whitesides. «The origins and the future of microfluidics». In: *nature* 442.7101 (2006), pp. 368–373 (cit. on p. 8).

[30] Sabo Wada Dutse and Nor Azah Yusof. «Microfluidics-based lab-on-chip systems in DNA-based biosensing: an overview». In: *Sensors* 11.6 (2011), pp. 5754–5768 (cit. on p. 8).

[31] Yanling Song, Bingqian Lin, Tian Tian, Xing Xu, Wei Wang, Qingyu Ruan, Jingjing Guo, Zhi Zhu, and Chaoyong Yang. «Recent progress in microfluidics-based biosensing». In: *Analytical chemistry* 91.1 (2018), pp. 388–404 (cit. on p. 8).

[32] Ahyeon Koh et al. «A soft, wearable microfluidic device for the capture, storage, and colorimetric sensing of sweat». In: *Science translational medicine* 8.366 (2016), 366ra165–366ra165 (cit. on p. 8).

[33] Nawab Singh, Md Azahar Ali, Prabhakar Rai, Ashutosh Sharma, BD Malhotra, and Renu John. «Microporous nanocomposite enabled microfluidic biochip for cardiac biomarker detection». In: *ACS applied materials & interfaces* 9.39 (2017), pp. 33576–33588 (cit. on p. 9).

[34] Luciano Babuin and Allan S Jaffe. «Troponin: the biomarker of choice for the detection of cardiac injury». In: *Cmaj* 173.10 (2005), pp. 1191–1202 (cit. on p. 10).

[35] Poomrat Rattanarat, Akkapol Suea-Ngam, Nipapan Ruecha, Weena Siangproh, Charles S Henry, Monpichar Srisa-Art, and Orawon Chailapakul. «Graphene-polyaniline modified electrochemical droplet-based microfluidic sensor for high-throughput determination of 4-aminophenol». In: *Analytica chimica acta* 925 (2016), pp. 51–60 (cit. on p. 10).

[36] Edward A Lock, Theresa J Cross, and Rick G Schnellmann. «Studies on the mechanism of 4-aminophenol-induced toxicity to renal proximal tubules». In: *Human & experimental toxicology* 12.5 (1993), pp. 383–388 (cit. on p. 11).

[37] Takeshi Kondo, Hironori Sakamoto, Takayoshi Kato, Masaru Horitani, Isao Shitanda, Masayuki Itagaki, and Makoto Yuasa. «Screen-printed diamond electrode: A disposable sensitive electrochemical electrode». In: *Electrochemistry communications* 13.12 (2011), pp. 1546–1549 (cit. on p. 12).

[38] Cristina Medina-Plaza, Celia Garcıa-Hernández, JA De Saja, JA Fernandez-Escudero, E Barajas, Germán Medrano, C Garcıa-Cabezón, Fernando Martin-Pedrosa, and Marıa Luz Rodriguez-Mendez. «The advantages of disposable screen-printed biosensors in a bioelectronic tongue for the analysis of grapes». In: *LWT-Food Science and Technology* 62.2 (2015), pp. 940–947 (cit. on p. 12).

[39] J-P Salvetat, J-M Bonard, NH Thomson, AJ Kulik, L Forro, W Benoit, and L Zuppiroli. «Mechanical properties of carbon nanotubes». In: *Applied Physics A* 69.3 (1999), pp. 255–260 (cit. on p. 14).

[40] J Hone, MC Llaguno, MJ Biercuk, AT Johnson, B Batlogg, Z Benes, and JE Fischer. «Thermal properties of carbon nanotubes and nanotube-based materials». In: *Applied physics A* 74.3 (2002), pp. 339–343 (cit. on p. 14).

[41] Chunyu Li, Erik T Thostenson, and Tsu-Wei Chou. «Sensors and actuators based on carbon nanotubes and their composites: a review». In: *Composites Science and Technology* 68.6 (2008), pp. 1227–1249 (cit. on p. 14).

[42] Vladimir Prelog. «Chirality in chemistry». In: *Croatica Chemica Acta* 79.3 (2006), pp. XLIX–LVII (cit. on p. 14).

[43] Nikhil Nandkumar. «Plasma—the fourth state of matter». In: *Int J Sci Technol Res* 3.9 (2014), pp. 49–52 (cit. on p. 14).

[44] A Belkind and S Gershman. «Plasma cleaning of surfaces». In: *Vacuum Coating and Technology November* (2008), pp. 46–57 (cit. on p. 14).

[45] Howard A Green, Yacov Domankevitz, and Norman S Nishioka. «Pulsed carbon dioxide laser ablation of burned skin: in vitro and in vivo analysis». In: *Lasers in surgery and medicine* 10.5 (1990), pp. 476–484 (cit. on p. 15).

[46] Judah Folkman. «Angiogenesis». In: *Biology of endothelial cells* (1984), pp. 412–428 (cit. on p. 16).

[47] Peter C Maisonpierre et al. «Angiopoietin-2, a natural antagonist for Tie2 that disrupts in vivo angiogenesis». In: *Science* 277.5322 (1997), pp. 55–60 (cit. on p. 16).

[48] Alexander Scholz, Karl H Plate, Yvonne Reiss, et al. «Angiopoietin-2: a multifaceted cytokine that functions in both angiogenesis and inflammation». In: *Ann NY Acad Sci* 1347.1 (2015), pp. 45–51 (cit. on p. 16).

[49] Xinqi Wu et al. «Angiopoietin-2 as a biomarker and target for immune checkpoint therapy». In: *Cancer immunology research* 5.1 (2017), pp. 17–28 (cit. on p. 16).

[50] Erica Villa et al. «Dynamic angiopoietin-2 assessment predicts survival and chronic course in hospitalized patients with COVID-19». In: *Blood advances* 5.3 (2021), pp. 662–673 (cit. on p. 16).

[51] Philippe Hantson, Papa N'Geye, Marie Laforge, Jean-Luc Clemessy, and Frédéric Baud. «Suicide attempt by ingestion of potassium ferricyanide». In: *Journal of Toxicology: Clinical Toxicology* 34.4 (1996), pp. 471–473 (cit. on p. 16).

[52] John Albert Newton Friend and William Nelson Smirles. «CCXCI.—The solubility of potassium ferricyanide in water between 0° and 100°». In: *Journal of the Chemical Society (Resumed)* (1928), pp. 2242–2245 (cit. on p. 16).

[53] A Bogomolova, E Komarova, K Reber, T Gerasimov, O Yavuz, S Bhatt, and M Aldissi. «Challenges of electrochemical impedance spectroscopy in protein biosensing». In: *Analytical Chemistry* 81.10 (2009), pp. 3944–3949 (cit. on p. 18).

[54] Woosung Choi, Heon-Cheol Shin, Ji Man Kim, Jae-Young Choi, and Won-Sub Yoon. «Modeling and applications of electrochemical impedance spectroscopy (EIS) for lithium-ion batteries». In: *Journal of Electrochemical Science and Technology* 11.1 (2020), pp. 1–13 (cit. on p. 18).

[55] E Casero, AM Parra-Alfambra, MD Petit-Domınguez, F Pariente, E Lorenzo, and C Alonso. «Differentiation between graphene oxide and reduced graphene by electrochemical impedance spectroscopy (EIS)». In: *Electrochemistry Communications* 20 (2012), pp. 63–66 (cit. on p. 19).

[56] Fu-Ming Wang and John Rick. «Synergy of Nyquist and Bode electrochemical impedance spectroscopy studies to commercial type lithium ion batteries». In: *Solid State Ionics* 268 (2014), pp. 31–34 (cit. on p. 19).

[57] Chih-Yu Lai, Wei-Chen Huang, Jui-Hong Weng, Lin-Chi Chen, Chia-Fu Chou, and Pei-Kuen Wei. «Impedimetric aptasensing using a symmetric Randles circuit model». In: *Electrochimica Acta* 337 (2020), p. 135750 (cit. on p. 19).

[58] C Heubner, M Schneider, and A Michaelis. «Investigation of charge transfer kinetics of Li-Intercalation in LiFePO4». In: *Journal of Power Sources* 288 (2015), pp. 115–120 (cit. on p. 20).

[59] M Schönleber, C Uhlmann, P Braun, A Weber, and E Ivers-Tiffée. «A consistent derivation of the impedance of a lithium-ion battery electrode and its dependency on the state-of-charge». In: *Electrochimica Acta* 243 (2017), pp. 250–259 (cit. on p. 20).

[60] Niazul I Khan and Edward Song. «Lab-on-a-chip systems for aptamer-based biosensing». In: *Micromachines* 11.2 (2020), p. 220 (cit. on p. 21).

[61] Emma J Hollick, David J Spalton, Paul G Ursell, and Milind V Pande. «Biocompatibility of poly (methyl methacrylate), silicone, and AcrySof intraocular lenses: randomized comparison of the cellular reaction on the anterior lens surface». In: *Journal of Cataract & Refractive Surgery* 24.3 (1998), pp. 361–366 (cit. on p. 24).

[62] Yiqiang Fan, Kexin Gao, Jie Chen, Wengang Li, and Yajun Zhang. «Low-cost PMMA-based microfluidics for the visualization of enhanced oil recovery». In: *Oil & Gas Science and Technology–Revue d'IFP Energies nouvelles* 73 (2018), p. 26 (cit. on p. 24).

[63] Marie–Claire Bélanger and Yves Marois. «Hemocompatibility, biocompatibility, inflammatory and in vivo studies of primary reference materials low-density polyethylene and polydimethylsiloxane: A review». In: *Journal of Biomedical Materials Research: An Official Journal of The Society for Biomaterials, The Japanese Society for Biomaterials, and The Australian Society for Biomaterials and the Korean Society for Biomaterials* 58.5 (2001), pp. 467–477 (cit. on p. 28).

[64] Navin Chand and SR Vashishtha. «Development, structure and strength properties of PP/PMMA/FA blends». In: *Bulletin of Materials Science* 23.2 (2000), pp. 103–107 (cit. on p. 29).

[65] Michael W Toepke and David J Beebe. «PDMS absorption of small molecules and consequences in microfluidic applications». In: *Lab on a Chip* 6.12 (2006), pp. 1484–1486 (cit. on p. 35).

[66] Valentin Mirceski and Rubin Gulaboski. «Recent achievements in square-wave voltammetry (a review)». In: *Macedonian Journal of Chemistry and Chemical Engineering* 33.1 (2014), pp. 1–12 (cit. on p. 35).

[67] JS Chen, J-P Diard, R Durand, and C Montella. «Hydrogen insertion reaction with restricted diffusion. Part 1. Potential step—EIS theory and review for the direct insertion mechanism». In: *Journal of Electroanalytical Chemistry* 406.1-2 (1996), pp. 1–13 (cit. on p. 35).

[68] Cheng-Hsin Chuang, Hsun-pei Wu, and Hung-Liang Chien. «Immunosensor with well-separated polyaniline nanowires for determination of isoelectric point based on electrochemical impedance spectroscopy». In: *The 9th IEEE International Conference on Nano/Micro Engineered and Molecular Systems (NEMS)*. IEEE. 2014, pp. 604–608 (cit. on pp. 38, 40).